



BIROn - Birkbeck Institutional Research Online

Exnicios, E.M. and Carter, Andrew and Najman, Y. and Clift, P.D. (2022) Late Miocene unroofing of the Inner Lesser Himalaya recorded in the NW Himalaya foreland basin. *Basin Research* 34 (6), pp. 1894-1916. ISSN 0950-091X.

Downloaded from: <https://eprints.bbk.ac.uk/id/eprint/52040/>

Usage Guidelines:

Please refer to usage guidelines at <https://eprints.bbk.ac.uk/policies.html> or alternatively contact lib-eprints@bbk.ac.uk.

1 **Late Miocene Unroofing of the Inner Lesser Himalaya Recorded in the**
2 **NW Himalaya Foreland Basin**

3
4 Elise M. Exnicios¹, Andrew Carter², Yani Najman³, Peter D. Clift^{1,4}

5
6 1 - Department of Geology and Geophysics, Louisiana State University, Baton Rouge, LA 70803,
7 USA

8 2 - Department of Earth and Planetary Sciences, Birkbeck College, University of London, London
9 WC1E 7HX, UK

10 3 - Lancaster Environment Centre, Lancaster University, Lancaster, LA1 4YQ, UK

11 4- Research Center for Earth System Science, Yunnan University, Kunming, Yunnan Province,
12 650091, PR China

13
14 **ABSTRACT:** Testing models that link climate and solid Earth tectonics in mountain belts requires
15 independent erosional, structural and climatic histories. Two well preserved stratigraphic sections
16 of the Himalayan foreland basin are exposed in NW India. The Jawalamukhi (13–5 Ma) and
17 Joginder Nagar sections (21–13 Ma) are dated by magnetostratigraphy and span a period of
18 significant climate change and tectonic evolution. We combine sediment geochemistry, detrital
19 zircon U-Pb dating, and apatite fission track analyses to reconstruct changes in the patterns of
20 erosion and exhumation in this area from the Early Miocene to Pliocene. The provenance of the
21 foreland sediments reflects a mixture of Tethyan and Greater Himalayan sources from 21 to 11
22 Ma, with influx from the Inner Lesser Himalaya starting after 11 Ma, and a strong increase in
23 Crystalline Inner Lesser Himalayan erosion after 8 Ma. This distinct shift in provenance most

24 likely reflects exhumation of the Kullu-Rampur Window, as well as the northward motion of the
25 Jawalamukhi section towards the Himalayas, drainage reorganization in the foreland, and/or
26 tectonically driven drainage capture in the mountains. Prior to 10.5 Ma sediment came from a
27 large river whose sources were Greater Himalaya and Haimanta dominated, likely a paleo-Sutlej,
28 while after 8 Ma the source river was dominated by a more local drainage. Our work is consistent
29 with Nd isotope and mica Ar-Ar constraints from the same sections that demonstrate initial Inner
30 Lesser Himalayan unroofing in this region from 11 Ma, earlier than the 2 Ma implied from the
31 marine record and during a period of summer monsoon weakening when fission track data indicate
32 very rapid cooling and erosion of the Lesser Himalaya sources from no later than 10 Ma.
33 Tectonically driven rock uplift coupled with southerly migration of the maximum rainfall belt
34 during a time of drying, may have focused erosion over the Lesser Himalayan Duplex and created
35 the Kullu-Rampur Window.

36

37 Keywords: Provenance, exhumation, Himalayas, monsoon, zircon

38

39 **1. Introduction**

40 What processes control the structural and topographic development of mountain chains?
41 Tectonic forces cause thickening of continental crust by folding and thrusting, driving uplift of the
42 Earth's surface, while extensional tectonics and erosion allow deep buried rocks to be brought to
43 the surface and topography to be flattened. It is increasingly recognized that the structure of
44 mountain belts reflects the interplay between these two competing forces, although much of our
45 understanding is derived from models rather than observations (Davis *et al.*, 1983; Beaumont *et*
46 *al.*, 2001; Willett *et al.*, 2003; Robinson *et al.*, 2006). These models suggest that focused erosion,
47 often caused by precipitation or glaciation in a restricted area, can drive asymmetric exhumation

48 and control the pattern of outcrop in compressional orogens. The Himalayas represent a classic
49 example of how climatic development, especially of the South Asian summer monsoon, might
50 interact with the structure and metamorphic history of a mountain chain (Wobus *et al.*, 2003;
51 Thiede *et al.*, 2004; Clift *et al.*, 2008).

52 Due to overprinting by metamorphism, subduction to great depths, and erosion of bedrock
53 once it reaches the surface, much of the record of an orogen's early history is typically lost from
54 the modern outcrop of the high ranges. Rocks now at the surface can only be used to reconstruct
55 the uplift and cooling of those particular units, but the older history of the Himalayas can only be
56 reconstructed from the erosional record preserved in the foreland basin and/or the deep-sea
57 submarine fans of the Indian Ocean (France-Lanord *et al.*, 1993; Clift *et al.*, 2001; Curray *et al.*,
58 2003; McNeill *et al.*, 2017).

59 Here we use new detrital zircon U-Pb dating and apatite fission analysis to explore the
60 links between tectonics, erosion and regional climate using a uniquely well-preserved sediment
61 record from the foreland basin in the NW Himalayas spanning >20 m.y. to test whether changes in
62 erosion patterns and rates are linked to variations in summer monsoon rains, or whether they might
63 instead be tied more closely to tectonic forces. We evaluate reconstructions for provenance
64 evolution derived from earlier work on the same sedimentary section: petrography and detrital
65 mica Ar-Ar dating that proposed a switch in the location of maximum erosion from the Greater
66 Himalaya (GHS) to either Tethyan Himalaya (THS)/Haimanta rocks (Fig. 1) (White *et al.*, 2002)
67 or Outer Lesser Himalayan (OLH) rocks (Colleps *et al.*, 2019) starting at 17 Ma; similar data and
68 bulk mudstone Nd and Sr isotopes were also used to propose an initial unroofing of the
69 unmetamorphosed Inner Lesser Himalaya (ILH) after 11 Ma and the Inner Lesser Himalayan
70 Crystalline Series (LHCS) after 6 Ma (Najman *et al.* (2009) and note correction in Najman *et al.*
71 (2010)). We note that the ILH structurally underlie the OLH so that the two units are sometimes

72 referred to as Lower and Upper LH by some workers, especially further east (Myrow *et al.*, 2015;
73 DeCelles *et al.*, 2016). In doing so we further explore the use of proximal foreland records
74 compared to regional submarine fan records in reconstructing the growth and erosion of orogenic
75 belts. The foreland offers the opportunity for significant sediment sequestration and later
76 reworking and resedimentation to a more distal location, complicating the source-to-sink transport
77 history and thus interpretation of marine sediments deposited at any given time. The proximal
78 records are also more able to sample limited stretches of the mountain front rather than integrating
79 the whole catchment. In doing so, foreland sediment can record along strike changes in erosion
80 and highlight details that are diluted beyond recognition in the deep sea fan.

81

82 **2. Regional Setting**

83 The Himalayas have formed as a result of continent-continent collision between India and
84 Eurasia, likely starting around ~55–50 Ma in the NW Himalayas (Green *et al.*, 2008; Najman *et*
85 *al.*, 2017) but potentially as recently as 34 Ma (Aitchison *et al.*, 2007) or even 20–25 Ma for
86 collision between the Indian craton and Eurasia (van Hinsbergen *et al.*, 2012)}. Collision in the
87 NW Himalayas may have slightly postdated collision in the central and eastern parts of the Indus-
88 Yarlung Suture Zone (DeCelles *et al.*, 2014; Wu *et al.*, 2014). The Himalayas consist of a number
89 of east-west striking, thrust-bound tectonic units, described, from south to north, below.

90 In the Sub-Himalayas of NW India and Pakistan, a Cenozoic marine to continental foreland
91 basin sequence is exposed, which comprises sedimentary rocks shed from the orogen (Parkash *et*
92 *al.*, 1980; Johnson *et al.*, 1985; Badgley & Tauxe, 1990; Sorkhabi & Arita, 1997; Ravikant *et al.*,
93 2011). These foreland sediments represent an invaluable archive of the early development of the
94 mountain belt (Meigs *et al.*, 1995; Burbank *et al.*, 1996; Najman, 2006) spanning important
95 climatic and environmental transitions, especially around 7–8 Ma when the climate dried, oceanic

96 upwelling increased and vegetation in the foreland shifted from being C3 to C4 dominated (Quade
97 *et al.*, 1989; Kroon *et al.*, 1991; Clift *et al.*, 2020; Zhou *et al.*, 2021), as well as more recently
98 identified older changes in wind and oceanography in the Arabian Sea starting around 11–13 Ma
99 (Gupta *et al.*, 2015; Bialik *et al.*, 2020).

100 The Sub-Himalayas represent the most southerly range within the orogen (Figs. 1 and 2),
101 The Neogene Siwalik Group to the south are separated from the older Dharamsala Group to the
102 north by the Palampur Thrust (Thakur *et al.*, 2010). In turn these are separated from the overriding
103 Lesser Himalayas (LH) by the Main Boundary Thrust (MBT), while they now overthrust
104 undeformed floodplains to the south along the Main Frontal Thrust (MFT). The LH can be divided
105 into two units, the Outer and Inner (Robinson *et al.*, 2001; Myrow *et al.*, 2015). The OLH
106 comprise Neoproterozoic to Cambrian sedimentary rocks believed to have been deposited on the
107 Indian passive margin synchronously with the sediments now forming the GHS (C  l  rier *et al.*,
108 2009; McKenzie *et al.*, 2011; Hughes, 2016). In contrast, the ILH range from Meso- and
109 Paleoproterozoic sedimentary rocks (Tewari, 2003; McKenzie *et al.*, 2011) to ~1.85 Ga schists and
110 gneisses of the LHCS (Miller *et al.*, 2000; Richards *et al.*, 2005).

111 The LHs are overthrust by the high-grade metamorphic rocks and leucogranites of the GHS
112 along the Main Central Thrust (MCT). The extensional South Tibet Detachment (STD) separates
113 the Tethyan Himalayan Series (THS), which and its higher-grade basal unit, the Haimanta Group,
114 from the underlying GHS (Frank *et al.*, 1995; Thakur & Tripathi, 2008). All of these units
115 represent rocks that were originally part of the Indian northern passive margin prior to collision,
116 with the GHS representing the result of the Cenozoic metamorphism associated with the orogeny.
117 The THS is back-thrusted towards the north on the Great Counter Thrust that places THS meta-
118 sedimentary rocks on top of the sequences of the Indus Suture Zone (Murphy & Yin, 2003; Yin,

119 2006), as well as the forearc to Eurasia, represented by the Indus Group in the NW Himalaya
120 (Brookfield & Andrews-Speed, 1984; Garzanti *et al.*, 1987; Henderson *et al.*, 2010).

121 The sedimentary section we study encompasses the time of exhumation of the LH, and we
122 therefore provide more detail on the evolution of this unit:

123 The LHs comprise an accretionary duplex whose origin may date back to ~20 Ma
124 (Bollinger *et al.*, 2004). The Tons Thrust that separates the ILH from the OLH is believed to have
125 been active by 16 Ma, with OLH exhumation after this time (Myrow *et al.*, 2015; Colleps *et al.*,
126 2019). Formation of a mid-crustal structural ramp at 11–12 Ma drove the duplexing of the ILH
127 (DeCelles *et al.*, 1998b), now exposed in the Kullu-Rampur Window (Colleps *et al.*, 2019), from
128 ~11 Ma (Thiede *et al.*, 2004; Vannay *et al.*, 2004; Caddick *et al.*, 2007) before the Pliocene LH
129 duplexing favored by Robinson *et al.* (2006) in western Nepal or that proposed by Webb (2013)
130 for the Kangra Embayment. Final emplacement of the LHs in the frontal ranges occurred as a
131 result of motion along the MBT. The timing of initiation of motion on the MBT has been assigned
132 to around 11 Ma along the entire Himalayan front (Meigs *et al.*, 1995), although when the first LH
133 rocks were finally exposed at the surface is debated. Deeken *et al.* (2011) have argued that the
134 MBT was active no later than 15 Ma in the area north of our studied sections. Changes in bulk
135 sediment isotopic signature imply that erosion of the ILH had begun in the front ranges by 10–11
136 Ma in Nepal (Huyghe *et al.*, 2010). Earlier work by Najman *et al.* (2009; 2010) in the same area as
137 our current study indicates that the distinctive ILH were first eroding from the Kullu-Rampur
138 Window by around 11 Ma. Colleps *et al.* (2019) preferred a date for this initial exposure at 3–7 Ma
139 in this NW Indian area, while favoring an older age of 9–11 Ma in Nepal (Fig. 2). Data from the
140 Indus submarine fan records the first significant input from the ILH at ~6 Ma, with a substantial
141 increase around 2–3 Ma (Clift *et al.*, 2019).

142 In the hinterland to our region of study, the LH are exposed along the range front in the
143 hanging wall of the MBT. It is not always clear whether these units are OLH or ILH. Webb (2013)
144 for example shows undifferentiated LH sedimentary rocks in the hanging wall within the Kangra
145 Embayment and OLH further to the east. Further north ILH are exposed within the tectonic Kullu-
146 Rampur Window (KRW) (Frank *et al.*, 1995) (Figs. 1 and 2) which breaches the GHS and
147 Haimanta. In the KRW, the ILH are composed of amphibolite facies early-mid Proterozoic
148 gneisses, schists and quartzites of the LHCS, which overthrust Mesoproterozoic un-
149 metamorphosed ILH phyllites, quartzites, carbonates and mafic volcanic rocks along the Munsiri
150 Thrust (Valdiya, 1980; Vannay & Grasemann, 1998; Thiede *et al.*, 2004). West of the KRW
151 Haimanta outcrops between the GHS and the range front thrust sheet of LH. According to Vannay
152 *et al.* (2004), after peak metamorphism at ~23 Ma, rapid exhumation of the GHS slowed in this
153 region after around 16 Ma, when movement along the MCT ceased. Peak metamorphic conditions
154 were no older than 11 Ma for the LHCS (Caddick *et al.*, 2007), after which time exhumation
155 occurred along the Munsiri Thrust, with the ILH of the KRW breaching surface in the late
156 Miocene-Early Pliocene (see also Colleps *et al.* (2019)).

157

158 **3. Summer Monsoon Variations**

159 The NW Himalayas are particularly suitable for testing links between climate and tectonics
160 because the region has one of the best long-term records of climatic evolution in Asia. Moreover,
161 the area is located on the edge of influence of the South Asian summer monsoon (Bookhagen &
162 Burbank, 2006) and thus is particularly sensitive to changes in the intensity and seasonality of the
163 rainfall. Although this area is also supplied by moisture during the winter via the Westerly Jet
164 (Karim & Veizer, 2002), the bulk of the rainfall, and especially the most erosive, stormy
165 precipitation events occur during the summer season (Bookhagen & Burbank, 2006). Summer

166 monsoon precipitation varies across the Indus catchment, broadly decreasing to the west from
167 ~507 mm (76% of the annual total) in Chandigarh (India), to 385 mm (64%) in Islamabad
168 (Pakistan) (www.weather-atlas.com). The Asian monsoon, spanning South and East Asia, is
169 believed to have strengthened due to building of high topography during the Himalayan orogeny
170 (Prell & Kutzbach, 1992; Molnar *et al.*, 1993; Boos & Kuang, 2010), although this may have
171 occurred in a number of phases of uplift and strengthening (Farnsworth *et al.*, 2019). Oceanic
172 upwelling driven by summer monsoon winds seems to have begun to intensify after 13 Ma (Gupta
173 *et al.*, 2015; Betzler *et al.*, 2016), with a subsequent increase after 11 Ma (Bialik *et al.*, 2020) and
174 another at 7–8 Ma (Kroon *et al.*, 1991; Prell *et al.*, 1992).

175 However, there is a disconnect between oceanic proxies and those related to continental
176 environmental conditions (Clift, 2017). While the transition from C3 tree-dominated flora to a
177 more C4-dominated grassy vegetation around 8 Ma was initially linked to monsoon intensification
178 (Quade *et al.*, 1989), this interpretation has since been reversed to imply Late Miocene drying
179 based on weathering intensity, oxygen isotopes in soil carbonates and the understanding that C4
180 grasses favor settings with strong dry seasons (Dettman *et al.*, 2001; Vögeli *et al.*, 2017a; Feakins
181 *et al.*, 2020). Hydrogen isotope data from leaf waxes extracted from marine sediments in the
182 Arabian Sea also show a progressive drying since 11 Ma (Huang *et al.*, 2007). This is also
183 consistent with chemical weathering data that demonstrates progressively less intense alteration
184 through time since the Late Miocene in sediments from the Indus Fan (Clift *et al.*, 2008; Clift &
185 Jonell, 2021b; Zhou *et al.*, 2021), although no clear temporal trend was seen in weathering proxies
186 in the sections considered here (Vögeli *et al.*, 2017b). Because chemical weathering rates are
187 generally considered to slow as moisture reduces and temperatures fall (Filippelli, 1997; West *et*
188 *al.*, 2005), weakening of the monsoon might be expected to cause less chemical weathering and
189 slower erosion, although slower sediment transport would have the opposite effect. The same

190 submarine fan sediments also show increasing amounts of hematite after 10 Ma (Zhou *et al.*,
191 2021), which is also suggestive of drying environments, or at least increasing seasonality
192 characterized by a prolonged dry season (Schwertmann, 1971).

193

194 **4. Previous Work**

195 *4.1 Foreland Basin Stratigraphy*

196 The Himalayan foreland sedimentary sequence spans much of the Cenozoic. Sections of
197 sedimentary rock from the foreland basin were progressively accreted into the mountains as the
198 Indian plate underthrust northward. Because of this, these sediments are preserved in the Sub-
199 Himalayan Siwalik hills (Fig. 1). Although the oldest part of the basin dates back to the Eocene
200 (Sahni & Srivastava, 1976; Najman, 2006; Ravikant *et al.*, 2011) there is a substantial
201 unconformity separating Paleogene rocks from the overlying Neogene, the latter forming the target
202 of this study (Najman *et al.*, 2004; Najman, 2006). It should be noted that some workers argue for
203 the section being more continuous and without a major break (Bera *et al.*, 2008), although new
204 geochronology data from Colleps *et al.* (2019) casts further doubt on this near continuous age
205 model. The stratigraphic sections exposed at Jawalamukhi and Joginder Nagar form the Sub-
206 Himalayan Neogene succession in our study area within the Kangra Embayment (Fig. 1). The
207 stratigraphic thickness of the Jawalamukhi section is ~3400 m, while the Joginder Nagar section is
208 ~2000 m thick (Fig. 3) (Meigs *et al.*, 1995; Brozovic & Burbank, 2000). Deposition of the
209 Dharamsala Formation in the Kangra Embayment during the Early to Middle Miocene was
210 followed by accumulation of the Middle Miocene to Lower Pleistocene Siwalik Group (Meigs *et*
211 *al.*, 1995; White *et al.*, 2002). The Joginder Nagar section is made up of the Dharamsala
212 Formation, which contains the Upper and Lower Dharamsala members. The Lower Dharamsala
213 Member comprises the older finer grained Chimnum (>20 Ma) and younger (17–20 Ma) coarser

214 grained Pabo formations (White *et al.*, 2002). The Upper Dharamsala Members comprises an older
215 finer grained Al Formation (15–17 Ma) and a younger coarser Makreri Formation (13–15 Ma).
216 The Jawalamukhi section comprises the Siwalik Group, encompassing the Upper, Middle, and
217 Lower Siwalik sub-groups. The combined sections represent a progressively coarsening-upward
218 sequence represented by fluvial sandstones, mostly of braided river origins passing up into
219 conglomerates of alluvial fan facies (Brozovic & Burbank, 2000; Najman *et al.*, 2009; 2010). The
220 depositional ages of these rocks have been constrained by magnetostratigraphy and radiometric
221 dating of detrital minerals that indicate maximum depositional age, allowing their correlation with
222 climate records (Meigs *et al.*, 1995; White *et al.*, 2001). The younger Jawalamukhi section spans
223 13–5 Ma and the Joginder Nagar section was deposited at 21–13 Ma (Fig. 3). Combined, these two
224 sections document the longest erosional and exhumation history available in the NW Himalayan
225 foreland (Burbank *et al.*, 1996).

226

227 *4.2 Earlier Provenance Work from the Joginder Nagar and Jawalamukhi sections*

228 Earlier studies of detrital monazite from the Dharamsala and Lower Siwalik Formations in
229 the Kangra Embayment indicated erosion of both high-grade GHS and similar protoliths such as
230 those preserved in the THS or OLH. The monazite also indicated erosion from Cambro-
231 Ordovician granites now found within the GHS and Haimanta Unit of the THS (White *et al.*,
232 2001). Further work on the same sections dating to 21–12.5 Ma included petrography, Sr-Nd
233 isotope bulk compositions and single-grain $^{40}\text{Ar}/^{39}\text{Ar}$ ages of mica (White *et al.*, 2002). This work,
234 particularly the short lag times determined from the predominance of Cenozoic micas, indicated
235 erosion from rapidly cooled GHS sources until ~17 Ma. This was followed by more erosion from a
236 lower grade source following cessation of motion on the MCT, as indicated by influx of older
237 mica grains and change in petrography; this source was considered to be the Haimanta of the THS

238 by White *et al.* (2002), reinterpreted as influx from the OLH by Colleps *et al.* (2019). Colleps *et*
239 *al.* (2019) used a combination of U-Pb and (U-Th)/He dating of zircons from both the LH and the
240 Dharamsala Group to identify a pulse of rapid exhumation along the Tons Thrust that separates the
241 OLH from the ILH at ~16 Ma. After ~12 Ma duplexing of the ILH shifted the locus of maximum
242 exhumation northward, allowing the rocks in the MCT hanging wall to be eroded and exposing the
243 ILH in the KRW. The upper part of the foreland sedimentary succession postdating 13 Ma near
244 Jawalamukhi was analyzed using the same methods by Najman *et al.* (2009; 2010). This work
245 implied initial erosion of the non-metamorphosed ILH after 11 Ma, based on the ϵ_{Nd} values of
246 clasts in pebbly sandstones; then loss of GHS drainage with material predominantly derived from
247 the Haimanta starting at 7 Ma, based on loss of Cenozoic micas; and then erosion from the LHCS
248 after 6 Ma based on a change to dominance of Precambrian micas.

249 Further to the east a multi-proxy study involving U-Pb zircon dating, bulk sediment
250 geochemistry and Sr-Nd isotopes targeted the Siwalik Group in the Dehra Dun region (Mandal *et*
251 *al.*, 2019). This work concluded that LHCS erosion started after 6 Ma, following ILH erosion
252 starting at least since 10 Ma, although erosion from the GHS and THS dominated. Erosion and
253 recycling of foreland sedimentary rocks intensified after 5.5 Ma probably because of southward
254 propagation of the thrust front from the MBT.

255

256 4.3 Rivers

257 The Indus River and its many tributaries are the main drainage system in the NW
258 Himalayan foreland (Fig. 2). The Beas River is an important tributary for this study because it is
259 located close to the sampled outcrops. Because the Siwaliks are offscraped and accreted parts of
260 the foreland the preserved sections must represent older equivalents of the modern floodplain,
261 potentially related to the Beas River since ongoing convergence necessarily brings Beas River

262 deposits towards the location of the preserved sections, where they might be offscraped in the
263 future, although axial rivers flowing further south might also be expected to contribute to older
264 parts of the preserved section. Although it has been argued that the eastern tributaries of the Indus
265 River used to flow to the east prior to the Late Miocene (Clift & Blusztajn, 2005), this model has
266 been questioned because it does not account for changing compositions through time of the
267 individual streams (Chirouze *et al.*, 2015).

268

269 **5. Methods**

270 13 sandstones were sampled from the Jawalamukhi and Joginder Nagar sedimentary
271 sections as shown in Figures 2 and 3, spanning the time range from 21 to 5 Ma (Table 1). We also
272 sampled the Beas River for a modern river sand for apatite fission track (AFT) work only. We use
273 a selection of bulk rock and single grain methods in order to constrain the source of the sediments.
274 Using a combination of different proxies allows the sediment source to be more accurately defined
275 and overcomes limitations in the resolution of individual methods. We use both high and low
276 temperature geo- and thermochronology to resolve between erosion from different source ranges,
277 as well as integrating pre-existing thermochronology and isotopic data taken from the same
278 section.

279

280 *5.1 X-Ray Fluorescence (XRF)*

281 Although erosion and sediment transport may result in changes in the bulk sediment
282 chemistry of deposited sediments compared with the pristine source rocks, major and trace
283 element chemistry of sedimentary rocks can be used to constrain their origin because some
284 elements are resistant to alteration and mobilization during diagenesis (McLennan *et al.*, 1993;
285 Fedo *et al.*, 1995; Singh, 2009). These data may also provide an image of the state of chemical

286 weathering through the section (Nesbitt *et al.*, 1980), which in turn may be linked to the monsoon
287 climate. The major element chemistry can show us large scale changes in sediment character that
288 provide context for the geochronology described below.

289 All thirteen whole rock sandstone samples were cut and processed through a jaw crusher.
290 The crushed rock samples were milled into fine grained powders. The powders were analyzed for
291 a suite of major elements and select trace elements through XRF spectrometry by the Washington
292 State University (WSU) GeoAnalytical Laboratory. Full analytical details are provided by Johnson
293 *et al.* (1999). Analytical uncertainties for major elements are ~1% of the measured value, as
294 determined from repeat analysis of a suite of nine USGS standard samples. Results are provided in
295 Table 2.

296

297 5.2 U-Pb Detrital Zircon Dating

298 Detrital zircon U-Pb dating was completed using laser ablation-multicollector-inductively
299 coupled plasma-mass spectrometry (LA-MC-ICP-MS). After separation of the zircon fraction by
300 standard heavy liquid methods by GeoSep Services of Moscow Idaho, the grains were mounted
301 and the U-Th-Pb isotopic compositions were determined at the London Geochronology Centre
302 facilities at University College London using a New Wave 193 nm aperture-imaged, frequency-
303 quintupled laser ablation system, coupled to an Agilent 7900 quadrupole-based ICP-MS. Full
304 methodology can be found in the Supplementary Information, along with all the isotopic analytical
305 data in Table S1.

306 We used kernel density estimates (KDEs) with pie charts to graphically display the detrital
307 age spectra and a multi-dimensional scalar (MDS) diagram to assess the degree of similarity
308 between samples (Vermeesch, 2013). Further modelling of the source contributions was made
309 using the DZMix Matlab routine of Sundell & Saylor (2017). This involves a Monte Carlo-based

310 mixing model, which allows the defined sources to the basin to be combined in order to try and
311 replicate the age spectra measured for each of the samples. 10,000 attempts are made to replicate
312 each particular detrital age spectrum through varying the contributions from the various sources in
313 order to match the observed age spectrum, with the best 1% selected (Figs. S1 and S2; Table S2 in
314 Online Supplement). This type of mixing can only be as good as the definition of the source areas,
315 although a large amount of bedrock data exists for the Himalayas. The ILH is distinctly different
316 from the OLH, THS and GHS concerning its U-Pb age spectrum. Because the OLH is the protolith
317 to the GHS, these two sources are indistinguishable in terms of their zircons age spectra. The
318 younger THS has a slightly different signature than the GHS and OLH, for example having a more
319 prominent ~500 Ma population and slightly fewer 900–1250 Ma grains, but it is mostly sourced
320 from these older units and therefore the differences are subtle. Therefore, we combine the OLH,
321 GHS and THS sources into one end member to allow a robust mixing model to be generated.

322 Furthermore, there is the added complexity that material that was originally derived from
323 one basement source might have been eroded and deposited temporarily elsewhere from where it
324 was then reworked into the flood plains (e.g., from the older Dharamsala Formation). Recycling
325 material out of older sedimentary sequences complicates the sediment unmixing and is known to
326 affect the modern rivers (Clift & Jonell, 2021a); however, quantitative estimates from the
327 Nepalese central Himalaya indicate that the load of the rivers in that area contains no more than
328 ~10% material recycled from the Siwalik Group (Lavé & Avouac, 2000). We thus do not include
329 these sedimentary rocks in our mixing models, because Siwalik end members cannot be used to
330 model other Siwalik sedimentary rocks. There is no simple way to remove this recycling effect,
331 but it might be expected to influence all our samples. We look for systematic major changes in
332 zircon age populations to quantify changes in provenance with the understanding that even
333 apparently unique peaks might be recycled through older sedimentary deposits.

334

335 5.3 Apatite Fission Track

336 We use AFT methodology to trace the exhumation history of the source region by looking
337 at how lag times (mineral cooling age minus depositional age) evolve through the section. The
338 approach has been effective at reconstructing erosion rates elsewhere in the Himalaya. Analysis of
339 AFT in Nepal suggested that parts of the section may be reset during burial, prior to later uplift
340 and exposure (van der Beek *et al.*, 2006). Studies of fission track in the Siwaliks of the NW
341 Himalayas have largely been restricted to zircon FT (Bernet *et al.*, 2006; Chirouze *et al.*, 2015),
342 although AFT data spanning the last 16 Ma is available for comparison from the Indus Fan (Zhou
343 *et al.*, 2020).

344 AFT data were collected from eight samples ranging from 5–19 Ma plus as well a single
345 modern river sand from the Beas River. Following mineral separation AFT analysis was
346 performed at the London Geochronology Centre using the external detector approach Full methods
347 can be found in Supplementary Information.

348

349 6. RESULTS

350 6.1 Major Element Chemistry

351 The major element chemistry indicates that these sediments are typical high SiO₂
352 sandstones ranging from 66.6% to 93.3%, average 80.8% SiO₂ after normalizing for volatile
353 content (Fig. 4). This compares with an average of 74.9% SiO₂ for modern Indus catchment
354 Himalayan tributaries. The sediments have low contents of water mobile alkali earth elements,
355 such as K₂O and Na₂O. Average contents are 1.84% and 0.75% respectively compared with 2.38%
356 and 1.06% for the modern tributaries (Alizai *et al.*, 2011). On the ternary plot of Fedo *et al.*
357 (1995)(Fig. 4A), the samples overlap with the analyses of Vögeli *et al.* (2017b) for the same

358 sections but show a coherent displacement to higher Chemical Index of Alteration (CIA) values
359 compared to the Quaternary Indus delta, shelf and canyon (Clift *et al.*, 2010; Li *et al.*, 2018), as
360 well as post 11 Ma turbidites from the Indus Fan (Zhou *et al.*, 2021). The sediments yield very
361 high Zr contents, averaging 209 ppm compared to 38 ppm for the modern rivers, with the nearest
362 streams, the Sutlej and the Beas, having only ~14 ppm (Alizai *et al.*, 2011). The contrast with the
363 Quaternary and older Indus Fan sediments is also clear on the diagram of Herron (1988) in which
364 the samples first analyzed in this study plot as arkose to sublitharenite rather than as wackes.

365

366 6.2 Detrital U-Pb Zircon

367 The age spectra of the detrital grains show a number of repeated common age populations
368 that are comparable to ages measured from basement source rocks (Fig. 5). The most common
369 populations range 400–750 Ma, 900–1250 Ma, 1700–2000 Ma and >2400 Ma. Grains deposited at
370 and before 8–9 Ma are dominated by the 750–1250 Ma population. There is little variation in age
371 composition from 20 to 11 Ma, although the oldest two samples deposited at 18–19 Ma and 20–21
372 Ma show very few 400–750 Ma grains. The zircon age spectra over the interval before 11 Ma are
373 most similar to the OLH, THS and GHS, and the modern Ravi River (Figs. 5 and 6). After 12 Ma,
374 samples show an appreciable increase in zircons in the range 1700–2000 Ma (Fig 5), typical of the
375 ILH, and samples younger than 8 Ma are distinctive in having a strong 1800–1900 Ma peak and
376 very few grains younger than 1700 Ma, similar to the modern Sutlej River, but unlike the Beas
377 River. None of the samples contain grains <200 Ma, which are associated with the Indus River and
378 to a lesser extent the Jhelum River (where the grains span ~10–200 Ma and are derived from the
379 Karakoram, Kohistan and Nanga Parbat (Alizai *et al.*, 2011)), or even grains dated ~30 Ma which
380 are common in the Siwalik Group at Dehra Dun, as well as the Ganges (Mandal *et al.*, 2019).
381 Given the lack of 30–200 Ma grains in our section, these 30 Ma zircons must come from

382 Oligocene intrusive rocks in the GHS which are uncommon in NW India west of Dehra Dun
383 (Steck, 2003)

384

385 *6.3 Apatite Fission Track*

386 The central age defined by the radial plots (Fig. S1 in Online Supplement) represents the
387 time at which the dominant bedrock sources cooled through the AFT partial annealing zone
388 (PAZ), assuming that the sedimentary rock itself has not been subjected to temperatures sufficient
389 for the AFT ages to be reset, since deposition. The Beas River sample is clearly not reset and has a
390 central age of 1.4 ± 0.1 Ma, dominated by a single population (Table 3). The four youngest
391 sedimentary rocks (5–9 Ma) yielded single AFT populations indicating very short lag times
392 (central ages within error of their depositional age; Fig. 7). AFT analysis showed that samples
393 older than 9–10 Ma have been partially to completely reset because (1) their central age is
394 significantly younger than their depositional age, and (2) the central age youngs down section,
395 which is typical of a reset section.

396

397 **7 Discussion**

398 *7.1 Major Element Chemistry*

399 The major element chemistry is consistent with erosion from typical upper continental
400 crustal sources, although the contrast with the modern rivers and with the older deposits in the
401 Arabian Sea indicates that these sedimentary rocks are generally more weathered than the
402 sediments that reached the final depocentre in the recent or older past. The greater degree of
403 alteration reflects both their long storage in the floodplains immediately after sedimentation, when
404 they would have been exposed to moisture and heat, as well as renewed alteration during
405 diagenesis and further weathering as the ranges were uplifted more recently and the sediments

406 were again exposed. The high proportion of Zr compared to the modern rivers is suggestive of the
407 sources being relatively enriched in zircon compared to other source regions within the Indus
408 catchment, especially those in the suture zone and Karakoram. Strong weathering and diagenesis
409 may also have broken down less robust phases and increased the proportion of zircon. The major
410 element chemistry is however not diagnostic in terms of limiting the bedrock sources.

411

412 *7.2 Detrital U-Pb Zircon*

413 As noted above (see Section 6.2), for samples deposited from 21–9 Ma the dominant
414 population (750–1250 Ma) is similar to those seen in the OLH, GHS and THS (Fig. 5), which
415 share a very similar zircon U-Pb signature (see Section 5.2). It is clear that most of the samples are
416 similar to one another and distinct from the Indus River and the ILH (Fig. 6 and S4). Because the
417 Indus derives its sediments largely from the Karakoram and other parts of the suture zone
418 (Garzanti *et al.*, 2005; Garzanti *et al.*, 2020), the contrast with a part of the Himalayan foreland
419 remote from the Indus mainstream is unsurprising.

420

421 *7.2.1 Transition after 11 Ma*

422 At 11–12 Ma there was an increase in the 1700–2000 Ma zircon population distinctive of
423 the ILH, with further increase up-section, especially after 8 Ma (Fig. 5). End member modelling
424 using DZMix also supports the relative increase in erosion from the ILH, starting after 11 Ma and
425 accelerating after 8 Ma (Fig. 8a). Although 1700–2000 Ma grains are also seen in the OLH, GHS
426 and THS they are relatively scarce in those rocks compared to 750–1250 Ma zircons. If these latter
427 units were sources of the increase in 1700–2000 Ma grains to the Jawalamukhi section, then we
428 would anticipate finding far greater proportions of zircons of this younger 750–1250 Ma
429 population; however, this is not the case. Input from the ILH starting from 11 Ma is consistent

430 with previous work in this area, which identified non-metamorphosed ILH input from the Nd
431 isotopic signature of pebbly sandstone clasts by that time (Najman *et al.*, 2010) (Fig. 8b).
432 However, this previous work was unable to determine relative proportions of such input as it was
433 based on clast data, unrepresentative of the section overall.

434 Moreover, this age is consistent with the evidence for ILH erosion obtained slightly further
435 to the east in the Dehra Dun area where zircons indicate initial unroofing of these units at least
436 since 10 Ma (Mandal *et al.*, 2019).

437

438 7.2.2 Transition after 8 Ma

439 The distinct increase in 1700–2000 Ma zircons at 7–8 Ma (Fig. 5), tracking towards the
440 ILH on the MDS plot (Fig. 6A) is coincident with the loss of mica grains dated <50 Ma (Najman
441 *et al.*, 2009), implying loss of erosion from the GHS. Dominance of Paleozoic and Mesozoic
442 micas at this time would suggest a continuing Haimanta contribution in addition to the ILH (Fig.
443 8e). A second switch in mica provenance by 6 Ma, when grains become entirely Precambrian, and
444 a major change in Sr-Nd values of bulk sediment to values typical of the ILH (Fig 8b), is
445 consistent with a major ILH contribution, as indicated by the zircon ages.

446 It is important to note that the OLH are not exposed in the Kangra Embayment or in the
447 KRW and are not drained by the Beas River. It is thus unlikely that the Siwalik sections would
448 have received sediment from OLH sources close to the range front. Sediment supply to the
449 sections must have been from a paleo-Sutlej, Beas or potentially a smaller local river.

450 In the Dehra Dun area there was no loss of erosion from the GHS as we see at
451 Jawalamukhi, implying that this section was deposited from a separate river. Figure 9 shows KDE
452 plots of synchronous of samples from the Mohand Rao section at Dehra Dun and the Jawalamukhi

453 section. The figure shows that the size of the populations between 400 and 1250 Ma remained high
454 at Dehra Dun after 8 Ma while these groupings contracted sharply at Jawalamukhi.

455

456 7.2.3 Causes of the Provenance Changes

457 The changes in provenance could reflect autogenic drainage reorganization in the flood
458 plain, and/or the motion of the section across the basin between different river flood plains.

459 Alternatively, changes in provenance could relate to the progressive unroofing of the KRW and
460 the addition of ILH material to this area.

461 Tectonic evolution of the region, as determined from bedrock data, may well explain the
462 provenance changes we observe in the foreland. Prograde metamorphism in the LHCS of the
463 KRW terminated at 11 Ma by tectonic exhumation along the Munsiri Thrust (Vannay *et al.*,
464 2004; Caddick *et al.*, 2007; Thiede *et al.*, 2009). Najman *et al.* (2009; 2010) interpreted the first
465 appearance of ILH material at 11 Ma in the Jawalamukhi section as the result of input of non-
466 metamorphosed ILH material associated with this exhumation event, followed by exhumation of
467 the LHCS by 6 Ma, as unroofing of the window progressed. This is in agreement with the
468 interpretation of Mandal *et al.* (2019), in which a provenance change in the Siwalik Group at
469 Dehra Dun at 6 Ma is interpreted as due to unroofing of the LHCS.

470 Alternatively, provenance evolution may reflect changes in the location of the sites relative
471 to the foreland rivers (Fig. 10). India has been moving towards the NNE throughout the Neogene
472 (Molnar & Stock, 2009; Copley *et al.*, 2010; Clark, 2012) and as a result each of the sections that
473 have been accreted into the thrust stack within the Kangra Embayment must have approached this
474 part of the thrust front from the SSW prior to their offscraping. The rate of convergence (Clark,
475 2012) and the estimated distance of each section at the time of sedimentation of the individual
476 samples are provided in Table 1 and can be used as a rough guide to where each sample was

477 deposited relative to the mountain front. Stevens & Avouac (2015), estimate that presently around
478 half of the total convergence between India and Eurasia is absorbed within the Himalaya, so we
479 make an approximation that the other half represents convergence between the foreland basin and
480 the mountain front, in order to reposition each of the samples at the time of their sedimentation.

481 We estimate the geology of the source areas at various critical times based on the
482 geological map of DiPietro & Pogue (2004). Although we use the structural reconstructions of
483 Colleps *et al.* (2019) as a guide to the progressive unroofing of the different basement units, we
484 adjust these models for unroofing based on the results of our provenance analysis, as set out above.

485 As each section moved towards the Himalayas with ongoing convergence, each section
486 would have been under the influence of different rivers with contrasting provenance at different
487 times (Fig. 10). The major rivers flow towards the SW and when the sites were in the distal
488 foredeep, far from the mountain front, they may have been affected by sedimentation from these
489 tributaries. As they got closer to the mountains, in the proximal foredeep, each section would have
490 the opportunity to be affected by more local rivers (e.g., the Beas), which themselves would have
491 been in a state of constant reorganization and migration.

492 Sediment older than 11 Ma was supplied by a river eroding the GHS and THS, similar to
493 the modern Ravi River. However, the Ravi drainage has evolved since this time and the direction
494 of flow from its NW location precludes this as being the source of the older sediments at
495 Jawalamukhi and Joginder Nagar. The location of the Sutlej makes it the most likely source of
496 sediment, although the provenance signature must have been quite different than the LH
497 dominance seen in the modern Sutlej (Alizai *et al.*, 2011). This is to be expected since the KRW
498 that dominates the modern river was not yet exposed at that time.

499 We infer that the younger part of the section is being supplied by a river which was
500 dominantly deriving its material from the ILH, probably related to the KRW. The MDS plot (Fig.

501 6) shows the younger samples are most like the modern Sutlej. It is noteworthy that the Sutlej
502 River basin contain significant exposures of the GHS and THS but has a zircon population
503 dominated by ILH sources because of climatically driven focused erosion (Alizai *et al.*, 2011).
504 Nevertheless, the ϵ_{Nd} value of the modern Sutlej (Clift *et al.*, 2002) indicates that there is a
505 proportion of material derived from the GHS or THS; therefore, because the detrital mica data
506 shows that GHS material was cut from the younger part of Jawalamukhi section (Najman *et al.*,
507 2009; 2010), it is more likely that the younger sediments of the Jawalamukhi section would have
508 been supplied by a small local river draining only as far as the KRW or the neighboring Uttarkashi
509 semi-window. The provenance transition after 8 Ma may reflect motion from the Sutlej flood
510 plains to the Beas flood plains. If it was the Beas River then this must have changed its provenance
511 significantly since 5–6 Ma.

512

513 7.2.4 Comparison with the Indus Fan

514 From this set of detrital zircon data, combined with previously published techniques, it can
515 be deduced that the unroofing of the ILH in the source regions to these sediments began by 11 Ma
516 and increased after 8 Ma. Prior to that time the foreland deposits at Jawalamukhi are mostly
517 derived from the GHS and/or THS (Haimanta), since at least ~21 Ma. Relative lack of 1700–2000
518 Ma zircons seen in the Indus submarine fan until ~2 Ma (Clift *et al.*, 2019), implies that most of
519 the Indus catchment had not exposed significant ILH bedrock until much later than inferred at
520 Jawalamukhi. Thus, the river that supplied the sediments we study from 11 to 2 Ma was deriving
521 its material from a catchment that was atypical of the wider area to the NW, or that its discharge
522 was greatly diluted by supply from contrasting rivers that were not so greatly eroding ILH sources.
523 The foreland sediments dated here between 11–2 Ma were however more similar to foreland
524 sediments found in the Dehra Dun area further east in showing major erosion from the ILH after

525 11 Ma (Mandal *et al.*, 2019) compared to those in the Indus Fan. Sediments at Dehra Dun differ
526 from Jawalamukhi in retaining a significant GHS and THS input since at least 11 Ma.

527

528 *7.3 Apatite Fission Track*

529 Figure 7 shows how the AFT ages of the samples measured in this study compare both
530 with their depositional ages, and with other data both further east in the Nepalese part of the
531 foreland basin, as well as in the Indian Ocean submarine fans. There is no suggestion of more than
532 one AFT age population in those samples (8–9 Ma, 6–7 Ma, and 5–6 Ma), whose central ages are
533 within error of the depositional age, and therefore not reset. Their younging up-section is typical of
534 erosion from a progressively exhuming hinterland. These samples have short lag times indicating
535 rapid exhumation of the source region.

536 By contrast, samples older than 9 Ma are considered to be reset because the AFT ages form
537 a single population with a central age resolvably younger than the depositional age derived from
538 magnetic stratigraphy. Most of the reset rocks in the oldest part of the Joginder Nagar section lie in
539 the hanging wall of the Palampur Thrust that initiated prior to the oldest reset age of ~7 Ma. This
540 is consistent with the idea that the Dharamsala Formation and Lower Siwalik section (Joginder
541 Nagar section) was accreted to the toe of the orogenic wedge after 11.5 Ma, which is the age of the
542 youngest sediment known from this section. We conclude that the Palampur Thrust must have
543 started motion between 7.0 and 11.5 Ma. The single reset 2.2 Ma AFT age south of the Palampur
544 Thrust reflects an episode of uplift and erosion of that section by 2.2 Ma, presumably on the MFT
545 or an associated splay.

546 The AFT ages themselves do not provide any provenance information, because bedrock
547 AFT data from the potential sources in the modern mountains do not allow us to infer what the
548 AFT ages were in the same ranges in the past. Although we cannot determine the timing of the

549 start of rapid exhumation because the older samples are reset, it is noteworthy that the occurrence
550 of very rapidly cooled sediments starting no later than 9–10 Ma encompasses the time of
551 increasing flux of ILH materials into the basin we study. Earlier studies suggest that erosion of the
552 THS and GHS was slower after ~16–17 Ma in this region (White *et al.*, 2001; Vannay *et al.*, 2004;
553 Thiede *et al.*, 2009), albeit getting faster again in the Dhauladar Range of Chamba after the start of
554 motion on the MBT after ~10 Ma (Deeken *et al.*, 2011; Thiede *et al.*, 2017). Our data support the
555 idea of rapid unroofing of the duplexed ILH and LHCS in the KRW starting at least by the Late
556 Miocene (~11 Ma), and particularly after 9 Ma, consistent with bedrock data from the ILH in the
557 KRW (Caddick *et al.*, 2007; Thiede *et al.*, 2009; Schlup *et al.*, 2011). Modelling of
558 thermochronology data from the Sutlej-Beas region suggests accelerating erosion from the KRW
559 after 7 Ma (Stübner *et al.*, 2018). We further note that this was a time of rapid regional
560 exhumation, as inferred from AFT studies of the Indus submarine fan (Zhou *et al.*, 2020), the
561 Bengal Fan (Huyghe *et al.*, 2020), as well as in the Nepalese part of the foreland (Bernet *et al.*,
562 2006; van der Beek *et al.*, 2006). Lag times are longer in the modern Beas River than in the
563 foreland sediment deposited between 9 and 6 Ma but because the sources are quite different from
564 the youngest Siwalik sedimentary rocks in this study (Fig. 6) we cannot infer a widespread
565 slowing of exhumation in this region since 5–6 Ma based on these new data.

566

567 **8. Climate-Tectonic Synthesis**

568 The relative importance of tectonics versus climate in the evolution of the Himalayas is
569 long-debated, with the relative influence of variations in thrust belt geometry and its implications
570 for topographic development and landsliding, versus wetter climates and associated increase in
571 erosion both cited as important controls (Robert *et al.*, 2011; Thiede & Ehlers, 2013; Godard *et al.*,
572 2014).

573 Rapid exhumation of the ILH duplex since 11 Ma, may be explained solely by tectonics which
574 could have driven surface uplift and so facilitated mass wasting on steep slopes (Mandal *et al.*,
575 2019). River incision of the ILH in the KRW may be linked to solid Earth tectonic processes, for
576 example the ramp geometry of the Main Himalayan Thrust (Eugster *et al.*, 2018; Colleps *et al.*,
577 2019). However, the substantial increase of ILH input after 8 Ma is also coincident with a time of
578 climatic transition (Quade *et al.*, 1989; Singh *et al.*, 2011). In the foreland basin there is a
579 transition from C3 tree-dominated to a C4 grass-dominated vegetation at this time interpreted to
580 reflect a general drying of the climate, or at least the development of a strong dry season (Dettman
581 *et al.*, 2001; Feakins *et al.*, 2020). This trend was confirmed in the sections studied here by Vögeli
582 *et al.* (2017a) indicating a climatic transition at 7–8 Ma involving drying and more seasonality in
583 the NW Himalayas after that time, which is a hallmark of the South Asian monsoon.

584 Various proxies suggest that the region was drying in the Late Miocene and that both
585 regional weathering and erosion were slowing in the Indus Basin as a result (Clift *et al.*, 2008;
586 Clift, 2017). However, that is not to say that more limited parts of the mountain front were
587 experiencing rapid erosion, especially the LH (Caddick *et al.*, 2007; Thiede *et al.*, 2009). It is
588 possible that the climate change would have caused the maximum rainfall band to migrate
589 southwards compared to its location when the summer monsoon was stronger and rain penetrated
590 deeper into the Himalayas during the Middle and Early Miocene. If climate was an important
591 driver of exhumation, we suggest a feedback whereby uplift caused by thrusting in the LH wedge
592 focused the rainfall by generating topography that focused orographic rainfall and allowed the LH
593 duplex to further build and then exhume (Thiede & Ehlers, 2013). This contrasts with the area
594 further NW in Chamba where the high ranges of the GHS form a rain shadow, reduce erosion and
595 prevent duplexing of the underlying ILH (Deeken *et al.*, 2011).

596

597 **9. Conclusions**

598 Our study highlights the importance of localized foreland sections to accompany regional
599 erosional reconstructions, which are based on submarine fan sequences, when trying to understand
600 the erosion of large mountain belts over tectonically significant periods of geological time (>10
601 m.y.). Our work is consistent with the idea of ongoing climate-tectonic coupling. While stronger
602 monsoon may have driven exhumation of the GHS, the weakening and migration of rainfall in the
603 Late Miocene could be associated with duplexing.

604 Evidence for appreciable erosion from the ILH starts around 11 Ma and increased
605 progressively after 8 Ma. ILH input after 11 Ma is consistent with timing of movement on the
606 MBT, as well as with onset of ILH duplexing. Najman *et al.* (2009; 2010) attributed the change
607 from 8 Ma to progressive uplift and unroofing of the rocks in the KRW, consistent with the timing
608 of the window's exhumation as determined from bedrock analyses (Colleps *et al.*, 2019). The loss
609 of GHS and Haimanta erosion could indicate drainage evolution in the foreland and supply from a
610 smaller river late in the accumulation of the section. Progressive motion of the Jawalamukhi
611 section towards the range front, and/or drainage reorganization in the foreland during the Late
612 Miocene may play a role in controlling which river was supplying the section prior to its accretion
613 into the toe of the orogenic wedge.

614 The Jawalamukhi section must have initially been in the floodplains of a major, likely
615 basin axial river which was eroding both LH rocks and GHS-THS sources, probably a paleo-
616 Sutlej. Both modern rivers are dominated by grains of LH origin (Alizai *et al.*, 2011) despite the
617 fact that GHS and THS rocks are widely exposed in their catchments. However, the almost
618 complete lack of Cenozoic micas in the youngest sediments suggests that a smaller transverse river
619 with no GHS/THS source is more appropriate.

620

622 **Acknowledgements**

623 PC is grateful for support from the Charles T. McCord Chair in Petroleum Geology at Louisiana
624 State University. GeoSep Services are thanked for their mineral separating. Data for this paper are
625 available from Mendeley Data (<https://data.mendeley.com>), doi: 10.17632/9gjmpbc443.1. Andrew
626 Carter performed the zircon dating and fission track analysis. Yani Najman collected the sample.
627 Elise Exnicios processed the samples. Peter Clift and Elise Exnicios made the figures and wrote
628 the initial draft to which Yani Najman contributed. Peter Clift and Yani Najman wrote the revised
629 draft. All authors contributed to the interpretation and final manuscript. The paper benefited from
630 review comments from Rasmus Thiede and an anonymous reviewer.

631

632

633 **REFERENCES**

- 634 AITCHISON, J.C., ALI, J.R. & DAVIS, A.S. (2007) When and Where Did India and Asia Collide?
635 *Journal of Geophysical Research*, **112**. doi:10.1029/2006JB004706.
- 636 ALIZAI, A., CARTER, A., CLIFT, P.D., VANLANINGHAM, S., WILLIAMS, J.C. & KUMAR, R. (2011)
637 Sediment Provenance, Reworking and Transport Processes in the Indus River by U–Pb
638 Dating of Detrital Zircon Grains. *Global and Planetary Change*, **76**, 33-55.
639 doi:10.1016/j.gloplacha.2010.11.008.
- 640 BADGLEY, C. & TAUXE, L. (1990) Paleomagnetic Stratigraphy and Time in Sediments: Studies in
641 Alluvial Siwalik Rocks of Pakistan. *The Journal of Geology*, **98**, 457-477.
642 doi:10.1086/629419.
- 643 BEAUMONT, C., JAMIESON, R.A., NGUYEN, M.H. & LEE, B. (2001) Himalayan Tectonics Explained
644 by Extrusion of a Low-Viscosity Crustal Channel Coupled to Focused Surface Denudation.
645 *Nature*, **414**, 738-742. doi:10.1038/414738a.
- 646 BERA, M.K., SARKAR, A., CHAKRABORTY, P.P., LOYAL, R.S. & SANYAL, P. (2008) Marine to
647 Continental Transition in Himalayan Foreland. *Geological Society of America Bulletin*.
648 doi:10.1130/B26265.1.
- 649 BERNET, M., VAN DER BEEK, P., PIK, R., HUYGHE, P., MUGNIER, J.-L., LABRIN, E. & SZULC, A.G.
650 (2006) Miocene to Recent Exhumation of the Central Himalaya Determined from
651 Combined Detrital Zircon Fission-Track and U/Pb Analysis of Siwalik Sediments, Western
652 Nepal. *Basin Research*, **18**, 393–412. doi: 10.1111/j.1365-2117.2006.00303.
- 653 BETZLER, C., EBERLI, G.P., KROON, D., WRIGHT, J.D., SWART, P.K., NATH, B.N., ALVAREZ-
654 ZARIKIAN, C.A., ALONSO-GARCÍA, M., BIALIK, O.M., BLÄTTLER, C.L., GUO, J.A., HAFFEN,
655 S., HOROZAI, S., INOUE, M., JOVANE, L., LANCI, L., LAYA, J.C., MEE, A.L.H., LÜDMANN, T.,
656 NAKAKUNI, M., NIINO, K., PETRUNY, L.M., PRATIWI, S.D., REIJMER, J.J.G., REOLID, J.,
657 SLAGLE, A.L., SLOSS, C.R., SU, X., YAO, Z. & YOUNG, J.R. (2016) The Abrupt Onset of the
658 Modern South Asian Monsoon Winds. *Scientific Reports*, **29838**. doi:10.1038/srep29838.
- 659 BIALIK, O.M., AUER, G., OGAWA, N.O., KROON, D., WALDMANN, N.D. & OHKOUCHI, N. (2020)
660 Monsoons, Upwelling, and the Deoxygenation of the Northwestern Indian Ocean in
661 Response to Middle to Late Miocene Global Climatic Shifts. *Paleoceanography and*
662 *Paleoclimatology*, **35**, e2019PA003762. doi:10.1029/2019PA003762.
- 663 BOLLINGER, L., AVOUAC, J.P., BEYSSAC, O., CATLOS, E.J., HARRISON, T.M., GROVE, M., GOFFE, B.
664 & SAPKOTA, S. (2004) Thermal Structure and Exhumation History of the Lesser Himalaya
665 in Central Nepal. *Tectonics*, **23**, 19. doi:10.1029/2003TC001564.
- 666 BOOKHAGEN, B. & BURBANK, D.W. (2006) Topography, Relief, and Trmm-Derived Rainfall
667 Variations Along the Himalaya. *Geophysical Research Letters*, **33**.
668 doi:10.1029/2006GL026037.
- 669 BOOS, W.R. & KUANG, Z. (2010) Dominant Control of the South Asian Monsoon by Orographic
670 Insulation Versus Plateau Heating. *Nature*, **463**, 218-222. doi:10.1038/nature08707.
- 671 BROOKFIELD, M.E. & ANDREWS-SPEED, C.P. (1984) Sedimentology, Petrography and Tectonic
672 Significance of the Shelf, Flysch and Molasse Clastic Deposits across the Indus Suture
673 Zone, Ladakh, Nw India. *Sedimentary Geology*, **40**, 249-286. doi:10.1016/0037-
674 0738(84)90011-3.
- 675 BROZOVIC, N. & BURBANK, D.W. (2000) Dynamic Fluvial Systems and Gravel Progradation in the
676 Himalayan Foreland. *GSA Bulletin*, **112**, 394-412. doi:10.1130/0016-
677 7606(2000)112<394:Dfsagp>2.0.Co;2.

- 678 BURBANK, D.W., BECK, R.A. & MULDER, T. (1996) The Himalayan Foreland Basin. In: *The*
679 *Tectonics of Asia* (Ed. by A. Yin & T. M. Harrison), 149–188. Cambridge University
680 Press, New York.
- 681 CADDICK, M.J., BICKLE, M.J., HARRIS, N.B.W., HOLLAND, T.J.B., HORSTWOOD, M.S.A., PARRISH,
682 R.R. & AHMAD, T. (2007) Burial and Exhumation History of a Lesser Himalayan Schist:
683 Recording the Formation of an Inverted Metamorphic Sequence in Nw India. *Earth and*
684 *Planetary Science Letters*, **264**, 375-390. doi:10.1016/j.epsl.2007.09.011.
- 685 CAWOOD, P.A., JOHNSON, M.R.W. & NEMCHIN, A.A. (2007) Early Palaeozoic Orogenesis Along
686 the Indian Margin of Gondwana: Tectonic Response to Gondwana Assembly. *Earth and*
687 *Planetary Science Letters*, **255**, 70-84. doi:10.1016/j.epsl.2006.12.006.
- 688 CÉLÉRIER, J., HARRISON, T.M., WEBB, A.A.G. & YIN, A. (2009) The Kumaun and Garwhal Lesser
689 Himalaya, India: Part 1. Structure and Stratigraphy. *GSA Bulletin*, **121**, 1262-1280.
690 doi:10.1130/b26344.1.
- 691 CHIROUZE, F., HUYGHE, P., CHAUVEL, C., VAN DER BEEK, P., BERNET, M. & MUGNIER, J.-L. (2015)
692 Stable Drainage Pattern and Variable Exhumation in the Western Himalaya since the
693 Middle Miocene. *Journal of Geology*, **123**, 1–20. doi:10.1086/679305.
- 694 CLARK, M.K. (2012) Continental Collision Slowing Due to Viscous Mantle Lithosphere Rather
695 Than Topography. *Nature*, **483**, 74-77. doi:10.1038/nature10848.
- 696 CLIFT, P.D., SHIMIZU, N., LAYNE, G., GAEDICKE, C., SCHLÜTER, H.U., CLARK, M.K. & AMJAD, S.
697 (2001) Development of the Indus Fan and Its Significance for the Erosional History of the
698 Western Himalaya and Karakoram. *Geological Society of America Bulletin*, **113**, 1039–
699 1051. doi:10.1130/0016-7606(2001)113<1039:DOTIFA>2.0.CO;2.
- 700 CLIFT, P.D., LEE, J.I., HILDEBRAND, P., SHIMIZU, N., LAYNE, G.D., BLUSZTAJN, J., BLUM, J.D.,
701 GARZANTI, E. & KHAN, A.A. (2002) Nd and Pb Isotope Variability in the Indus River
702 System; Implications for Sediment Provenance and Crustal Heterogeneity in the Western
703 Himalaya. *Earth and Planetary Science Letters*, **200**, 91-106. doi:10.1016/S0012-
704 821X(02)00620-9.
- 705 CLIFT, P.D. & BLUSZTAJN, J.S. (2005) Reorganization of the Western Himalayan River System
706 after Five Million Years Ago. *Nature*, **438**, 1001-1003. doi:10.1038/nature04379.
- 707 CLIFT, P.D., HODGES, K., HESLOP, D., HANNIGAN, R., HOANG, L.V. & CALVES, G. (2008) Greater
708 Himalayan Exhumation Triggered by Early Miocene Monsoon Intensification. *Nature*
709 *Geoscience*, **1**, 875-880. doi:10.1038/ngeo351.
- 710 CLIFT, P.D., GIOSAN, L., CARTER, A., GARZANTI, E., GALY, V., TABREZ, A.R., PRINGLE, M.,
711 CAMPBELL, I.H., FRANCE-LANORD, C., BLUSZTAJN, J., ALLEN, C., ALIZAI, A., LÜCKGE, A.,
712 DANISH, M. & RABBANI, M.M. (2010) Monsoon Control over Erosion Patterns in the
713 Western Himalaya: Possible Feed-Backs into the Tectonic Evolution. In: *Monsoon*
714 *Evolution and Tectonic-Climate Linkage in Asia* (Ed. by P. D. Clift, R. Tada & H. Zheng),
715 *Special Publication*, **342**, 181–213. Geological Society, London.
- 716 CLIFT, P.D. (2017) Cenozoic Sedimentary Records of Climate-Tectonic Coupling in the Western
717 Himalaya. *Progress in Earth and Planetary Science*, **4**. doi:10.1186/s40645-017-0151-8.
- 718 CLIFT, P.D., ZHOU, P., STOCKLI, D.F. & BLUSZTAJN, J. (2019) Regional Pliocene Exhumation of
719 the Lesser Himalaya in the Indus Drainage. *Solid Earth*, **10**, 647-661. doi:10.5194/se-10-
720 647-2019.
- 721 CLIFT, P.D., KULHANEK, D.K., ZHOU, P., BOWEN, M.G., VINCENT, S.M., LYLE, M. & HAHN, A.
722 (2020) Chemical Weathering and Erosion Responses to Changing Monsoon Climate in the
723 Late Miocene of Southwest Asia. *Geological Magazine*, **157**, 939-955.
724 doi:10.1017/S0016756819000608.

- 725 CLIFT, P.D. & JONELL, T.N. (2021a) Monsoon Controls on Sediment Generation and Transport:
 726 Mass Budget and Provenance Constraints from the Indus River Catchment, Delta and
 727 Submarine Fan over Tectonic and Multi-Millennial Timescales. *Earth-Science Reviews*,
 728 103682. doi:10.1016/j.earscirev.2021.103682.
- 729 CLIFT, P.D. & JONELL, T.N. (2021b) Himalayan-Tibetan Erosion Is Not the Cause of Neogene
 730 Global Cooling. *Geophysical Research Letters*, **n/a**, e2020GL087742.
 731 doi:10.1029/2020GL087742.
- 732 COLLEPS, C.L., STOCKLI, D.F., MCKENZIE, N.R., WEBB, A.A.G. & HORTON, B.K. (2019) Neogene
 733 Kinematic Evolution and Exhumation of the Nw India Himalaya: Zircon Geo- and
 734 Thermochronometric Insights from the Fold-Thrust Belt and Foreland Basin. *Tectonics*, **38**,
 735 2059-2086. doi:10.1029/2018tc005304.
- 736 COPLEY, A., AVOUAC, J.-P. & ROYER, J.-Y. (2010) The India-Asia Collision and the Cenozoic
 737 Slowdown of the Indian Plate; Implications for the Forces Driving Plate Motions. *Journal*
 738 *of Geophysical Research*, **115**. doi:10.1029/2009JB006634.
- 739 CORRIGAN, J.D. & CROWLEY, J.L. (1990) Fission Track Analysis of Detrital Apatites from Sites
 740 717 and 718, Leg 116, Central Indian Ocean. *Proceedings of the Ocean Drilling Program*,
 741 *Scientific Results*, **116**, 75–92. doi:10.2973/odp.proc.sr.116.118.1990.
- 742 CURRAY, J.R., EMMEL, F.J. & MOORE, D.G. (2003) The Bengal Fan: Morphology, Geometry,
 743 Stratigraphy, History and Processes. *Marine and Petroleum Geology*, **19**, 1191–1223.
 744 doi:10.1016/S0264-8172(03)00035-7.
- 745 DAVIS, D., SUPPE, J. & DAHLEN, F.A. (1983) Mechanics of Fold-and-Thrust Belts and
 746 Accretionary Wedges. *Journal of Geophysical Research: Solid Earth*, **88**, 1153-1172.
 747 doi:10.1029/JB088iB02p01153.
- 748 DECELLES, P.G., GEHRELS, G.E., QUADE, J. & OJHA, T.P. (1998a) Eocene-Early Miocene Foreland
 749 Basin Development and the History of Himalayan Thrusting, Western and Central Nepal.
 750 *Tectonics*, **17**, 741-765. doi:10.1029/98tc02598.
- 751 DECELLES, P.G., GEHRELS, G.E., QUADE, J., OJHA, T.P., KAPP, P.A. & UPRETI, B.N. (1998b)
 752 Neogene Foreland Basin Deposits, Erosional Unroofing, and the Kinematic History of the
 753 Himalayan Fold-Thrust Belt, Western Nepal. *Geological Society of America Bulletin*, **110**,
 754 2-21. doi:10.1130/0016-7606(1998)110<0002:NFBDEU>2.3.CO;2.
- 755 DECELLES, P.G., GEHRELS, G.E., QUADE, J., LAREAU, B. & SPURLIN, M. (2000) Tectonic
 756 Implications of U-Pb Zircon Ages of the Himalayan Orogenic Belt in Nepal. *Science*, **288**,
 757 497-499. doi:10.1126/science.288.5465.497.
- 758 DECELLES, P.G., GEHRELS, G.E., NAJMAN, Y., MARTIN, A.J., CARTER, A. & GARZANTI, E. (2004)
 759 Detrital Geochronology and Geochemistry of Cretaceous–Early Miocene Strata of Nepal:
 760 Implications for Timing and Diachroneity of Initial Himalayan Orogenesis. *Earth and*
 761 *Planetary Science Letters*, **227**, 313-330. doi:10.1016/j.epsl.2004.08.019.
- 762 DECELLES, P.G., KAPP, P., GEHRELS, G.E. & DING, L. (2014) Paleocene-Eocene Foreland Basin
 763 Evolution in the Himalaya of Southern Tibet and Nepal: Implications for the Age of Initial
 764 India-Asia Collision. *Tectonics*, **33**, 824–849. doi:10.1002/2014TC003522.
- 765 DECELLES, P.G., CARRAPA, B., GEHRELS, G.E., CHAKRABORTY, T. & GHOSH, P. (2016) Along-
 766 Strike Continuity of Structure, Stratigraphy, and Kinematic History in the Himalayan
 767 Thrust Belt: The View from Northeastern India. *Tectonics*, **35**, 2995–3027.
 768 doi:10.1002/2016TC004298.
- 769 DEEKEN, A., THIEDE, R.C., SOBEL, E.R., HOURIGAN, J.K. & STRECKER, M.R. (2011) Exhumational
 770 Variability within the Himalaya of Northwest India. *Earth and Planetary Science Letters*,
 771 **305**, 103-114. doi:10.1016/j.epsl.2011.02.045.

- 772 DETTMAN, D.L., KOHN, M.J., QUADE, J., RYERSON, F.J., OJHA, T.P. & HAMIDULLAH, S. (2001)
773 Seasonal Stable Isotope Evidence for a Strong Asian Monsoon Throughout the Past 10.7
774 M.Y. *Geology*, **29**, 31-34. doi:10.1130/0091-7613(2001)029<0031:SSIEFA>2.0.CO;2.
- 775 DIPIETRO, J.A. & POGUE, K.R. (2004) Tectonostratigraphic Subdivisions of the Himalaya: A View
776 from the West. *Tectonics*, **23**. doi:10.1029/2003TC001554.
- 777 EUGSTER, P., THIEDE, R.C., SCHERLER, D., STÜBNER, K., SOBEL, E.R. & STRECKER, M.R. (2018)
778 Segmentation of the Main Himalayan Thrust Revealed by Low-Temperature
779 Thermochronometry in the Western Indian Himalaya. *Tectonics*, **37**, 2710-2726.
780 doi:10.1029/2017TC004752.
- 781 FARNSWORTH, A., LUNT, D.J., ROBINSON, S.A., VALDES, P.J., ROBERTS, W.H.G., CLIFT, P.D.,
782 MARKWICK, P., SU, T., WROBEL, N., BRAGG, F., KELLAND, S.-J. & PANCOST, R.D. (2019)
783 Past East Asian Monsoon Evolution Controlled by Paleogeography, Not
784 Co≪Sub≫2≪/Sub≫. *Science Advances*, **5**, eaax1697.
785 doi:10.1126/sciadv.aax1697.
- 786 FEAKINS, S.J., LIDDY, H.M., TAUXE, L., GALY, V., FENG, X., TIERNEY, J.E., MIAO, Y. & WARNY, S.
787 (2020) Miocene C4 Grassland Expansion as Recorded by the Indus Fan.
788 *Paleoceanography and Paleoclimatology*, **35**, e2020PA003856.
789 doi:10.1029/2020PA003856.
- 790 FEDO, C.M., NESBITT, H.W. & YOUNG, G.M. (1995) Unraveling the Effects of Potassium
791 Metasomatism in Sedimentary Rocks and Paleosols, with Implications for Paleoweathering
792 Conditions and Provenance. *Geology*, **23**, 921–924. doi:10.1130/0091-
793 7613(1995)023<0921:UTEOPM>2.3.CO;2.
- 794 FILIPPELLI, G.M. (1997) Intensification of the Asian Monsoon and a Chemical Weathering Event
795 in the Late Miocene-Early Pliocene: Implications for Late Neogene Climate Change.
796 *Geology*, **25**, 27-30. doi:10.1130/0091-7613(1997)025<0027:IOTAMA>2.3.CO;2.
- 797 FRANCE-LANORD, C., DERRY, L. & MICHARD, A. (1993) Evolution of the Himalaya since Miocene
798 Time: Isotopic and Sedimentologic Evidence from the Bengal Fan In: *Himalayan*
799 *Tectonics* (Ed. by P. J. Treloar & M. P. Searle), *Special Publications*, **74**, 603–621.
800 Geological Society, London.
- 801 FRANK, W., GASEMANN, B., GUNTALI, P. & MILLER, C. (1995) Geological Map of the Kishtwar-
802 Chamba-Kulu Region (Nw Himalayas, India). *Jahrbuch der Geologischen Bundesanstalt*,
803 **138**, 299-308.
- 804 GALBRAITH, R.F. (1990) The Radial Plot: Graphical Assessment of Spread in Ages *Nuclear*
805 *Tracks and Radiation Measurement*, **17**, 207–214. doi:10.1016/1359-0189(90)90036-W.
- 806 GARZANTI, E., BAUD, A. & MASCLE, G. (1987) Sedimentary Record of the Northward Flight of
807 India and Its Collision with Eurasia (Ladakh Himalaya, India). *Geodinamica Acta*, **1**, 297–
808 312. doi:10.1080/09853111.1987.11105147.
- 809 GARZANTI, E., VEZZOLI, G., ANDO, S., PAPARELLA, P. & CLIFT, P.D. (2005) Petrology of Indus
810 River Sands; a Key to Interpret Erosion History of the Western Himalayan Syntaxis. *Earth*
811 *and Planetary Science Letters*, **229**, 287-302. doi: 10.1016/j.epsl.2004.11.008.
- 812 GARZANTI, E., LIANG, W., ANDÒ, S., CLIFT, P.D., RESENTINI, A., VERMEESCH, P. & VEZZOLI, G.
813 (2020) Provenance of Thal Desert Sand: Focused Erosion in the Western Himalayan
814 Syntaxis and Foreland-Basin Deposition Driven by Latest Quaternary Climate Change.
815 *Earth-Science Reviews*, **207**, 103220. doi:10.1016/j.earscirev.2020.103220.
- 816 GEHRELS, G., KAPP, P., DECELLES, P., PULLEN, A., BLAKEY, R., WEISLOGEL, A., DING, L., GUYNN,
817 J., MARTIN, A., MCQUARRIE, N. & YIN, A. (2011) Detrital Zircon Geochronology of Pre-

- 818 Tertiary Strata in the Tibetan-Himalayan Orogen. *Tectonics*, **30**, TC5016.
819 doi:10.1029/2011tc002868.
- 820 GEHRELS, G.E., DECELLES, P.G., OJHA, T.P. & UPRETI, B.N. (2006) Geologic and U-Th-Pb
821 Geochronologic Evidence for Early Paleozoic Tectonism in the Kathmandu Thrust Sheet,
822 Central Nepal Himalaya. *Geological Society of America Bulletin*, **118**, 185-198.
823 doi:10.1130/b25753.1.
- 824 GODARD, V., BOURLÈS, D.L., SPINABELLA, F., BURBANK, D.W., BOOKHAGEN, B., FISHER, G.B.,
825 MOULIN, A. & LÉANNI, L. (2014) Dominance of Tectonics over Climate in Himalayan
826 Denudation. *Geology*, **42**, 243-246. doi:10.1130/g35342.1.
- 827 GREEN, O.R., SEARLE, M.P., CORFIELD, R.I. & CORFIELD, R.M. (2008) Cretaceous-Tertiary
828 Carbonate Platform Evolution and the Age of the India-Asia Collision Along the Ladakh
829 Himalaya (Northwest India). *Journal of Geology*, **116**, 331–353. doi: 10.1086/588831.
- 830 GUPTA, A.K., YUVARAJA, A., PRAKASAM, M., CLEMENS, S.C. & VELU, A. (2015) Evolution of the
831 South Asian Monsoon Wind System since the Late Middle Miocene. *Palaeogeography,*
832 *Palaeoclimatology, Palaeoecology*, **438**, 160–167. doi:10.1016/j.palaeo.2015.08.006.
- 833 HENDERSON, A.L., NAJMAN, Y., PARRISH, R., BOUDAGHER-FADEL, M., BARFORD, D., GARZANTI,
834 E. & ANDÒ, S. (2010) Geology of the Cenozoic Indus Basin Sedimentary Rocks:
835 Paleoenvironmental Interpretation of Sedimentation from the Western Himalaya During
836 the Early Phases of India-Eurasia Collision *Tectonics*, **29**. doi:10.1029/2009TC002651.
- 837 HERRON, M.M. (1988) Geochemical Classification of Terrigenous Sands and Shales from Core or
838 Log Data. *Journal of Sedimentary Petrology*, **58**, 820–829. doi:10.1306/212F8E77-2B24-
839 11D7-8648000102C1865D.
- 840 HORTON, F. & LEECH, M.L. (2013) Age and Origin of Granites in the Karakoram Shear Zone and
841 Greater Himalaya Sequence, Nw India. *Lithosphere*, **5**, 300-320. 10.1130/l213.1.
- 842 HUANG, Y., CLEMENS, S.C., LIU, W., WANG, Y. & PRELL, W.L. (2007) Large-Scale Hydrological
843 Change Drove the Late Miocene C4 Plant Expansion in the Himalayan Foreland and
844 Arabian Peninsula. *Geology*, **35**, 531-534. doi:10.1130/G23666A.1.
- 845 HUGHES, N.C. (2016) The Cambrian Palaeontological Record of the Indian Subcontinent. *Earth-*
846 *Science Reviews*, **159**, 428-461. doi:10.1016/j.earscirev.2016.06.004.
- 847 HURFORD, A. (1990) Standardization of Fission Track Dating Calibration: Recommendation by the
848 Fission Track Working Group of the Iugs Subcommittee on Geochronology. *Chemical*
849 *Geology*, **80**, 177–178. doi:10.1016/0168-9622(90)90025-8.
- 850 HUYGHE, P., GUILBAUD, R., BERNET, M., GALY, A. & GAJUREL, A.P. (2010) Significance of the
851 Clay Mineral Distribution in Fluvial Sediments of the Neogene to Recent Himalayan
852 Foreland Basin (West-Central Nepal). *Basin Research*, **22**. doi: 10.1111/j.1365-
853 2117.2010.00485.x.
- 854 HUYGHE, P., BERNET, M., GALY, A., NAYLOR, M., CRUZ, J., GYAWALI, B.R., GEMIGNANI, L. &
855 MUGNIER, J.L. (2020) Rapid Exhumation since at Least 13 Ma in the Himalaya Recorded
856 by Detrital Apatite Fission-Track Dating of Bengal Fan (Iodp Expedition 354) and Modern
857 Himalayan River Sediments. *Earth and Planetary Science Letters*, **534**, 116078.
858 doi:10.1016/j.epsl.2020.116078.
- 859 JOHNSON, D., HOOPER, P. & CONREY, R. (1999) Xrf Method Xrf Analysis of Rocks and Minerals
860 for Major and Trace Elements on a Single Low Dilution Li-Tetraborate Fused Bead. *Adv.*
861 *X-ray anal*, **41**, 843-867.
- 862 JOHNSON, N.M., STIX, J., TAUXE, L., CERVENY, P.F. & TAHIRKHELI, R.A.K. (1985) Palaeomagnetic
863 Chronology, Fluvial Processes and Tectonic Implications of the Siwalik Deposits near
864 Chinji Village, Pakistan. *Journal of Geology*, **93**, 27–40. doi:10.1086/628917.

- 865 JONELL, T.N., CARTER, A., BÖNING, P., PAHNKE, K. & CLIFT, P.D. (2017) Climatic and Glacial
866 Impact on Erosion Patterns and Sediment Provenance in the Himalayan Rain Shadow,
867 Zanskar River, Nw India. *Geological Society of America Bulletin*, **129**, 820-836.
868 doi:10.1130/b31573.1.
- 869 KARIM, A. & VEIZER, J. (2002) Water Balance of the Indus River Basin and Moisture Source in the
870 Karakoram and Western Himalayas: Implications from Hydrogen and Oxygen Isotopes
871 River Water. *Journal of Geophysical Research*, **107**. doi:10.1029/2000JD000253.
- 872 KOHN, M.J., PAUL, S.K. & CORRIE, S.L. (2009) The Lower Lesser Himalayan Sequence: A
873 Paleoproterozoic Arc on the Northern Margin of the Indian Plate. *Geological Society of
874 America Bulletin*, **122**, 323-335. doi:10.1130/b26587.1.
- 875 KROON, D., STEENS, T. & TROELSTRA, S.R. (1991) Onset of Monsoonal Related Upwelling in the
876 Western Arabian Sea as Revealed by Planktonic Foraminifers. In: *Proceedings of the
877 Ocean Drilling Program, Scientific Results* (Ed. by W. Prell & N. Niitsuma), **117**, 257–
878 263. Ocean Drilling Program, College Station, TX.
- 879 LAVÉ, J. & AVOUAC, J.P. (2000) Active Folding of Fluvial Terraces across the Siwaliks Hills
880 (Himalayas of Central Nepal). *Journal of Geophysical Research*, **105**, 5735–5770. doi:
881 10.1029/1999JB900292.
- 882 LI, Y., CLIFT, P.D., BÖNING, P., BLUSZTAJN, J., MURRAY, R.W., IRELAND, T., PAHNKE, K., HELM,
883 N.C. & GIOSAN, L. (2018) Continuous Holocene Input of River Sediment to the Indus
884 Submarine Canyon. *Marine Geology*, **406**, 159-176. doi:10.1016/j.margeo.2018.09.011.
- 885 MANDAL, S.K., SCHERLER, D., ROMER, R.L., BURG, J.-P., GUILLONG, M. & SCHLEICHER, A.M.
886 (2019) Multiproxy Isotopic and Geochemical Analysis of the Siwalik Sediments in Nw
887 India: Implication for the Late Cenozoic Tectonic Evolution of the Himalaya. *Tectonics*,
888 **38**, 120-143. doi:10.1029/2018TC005200.
- 889 MARTIN, A.J., DECELLES, P.G., GEHRELS, G.E., PATCHETT, P.J. & ISACHSEN, C. (2005) Isotopic
890 and Structural Constraints on the Location of the Main Central Thrust in the Annapurna
891 Range, Central Nepal Himalaya. *Geological Society of America Bulletin*, **117**.
892 doi:10.1130/b25646.1.
- 893 MARTIN, A.J., GANGULY, J. & DECELLES, P.G. (2009) Metamorphism of Greater and Lesser
894 Himalayan Rocks Exposed in the Modi Khola Valley, Central Nepal. *Contributions to
895 Mineralogy and Petrology*, **159**, 203-223. doi:10.1007/s00410-009-0424-3.
- 896 MCKENZIE, N.R., HUGHES, N.C., MYROW, P.M., XIAO, S. & SHARMA, M. (2011) Correlation of
897 Precambrian–Cambrian Sedimentary Successions across Northern India and the Utility of
898 Isotopic Signatures of Himalayan Lithotectonic Zones. *Earth and Planetary Science
899 Letters*, **312**, 471-483. doi:10.1016/j.epsl.2011.10.027.
- 900 MCLENNAN, S., HEMMING, S., MCDANIEL, D. & HANSON, G. (1993) Geochemical Approaches to
901 Sedimentation, Provenance, and Tectonics (Ed. by M. J. Johnson & A. Basu), *Special
902 Papers*, **284**, 21-21. Geological Society of America, Boulder. doi:10.1130/SPE284-p21.
- 903 MCNEILL, L.C., DUGAN, B., BACKMAN, J., PICKERING, K.T., POUDEIROUX, H.F.A., HENSTOCK, T.J.,
904 PETRONOTIS, K.E., CARTER, A., CHEMALE, F., MILLIKEN, K.L., KUTTEROLF, S.,
905 MUKOYOSHI, H., CHEN, W., KACHOVICH, S., MITCHISON, F.L., BOURLANGE, S., COLSON,
906 T.A., FREDERIK, M.C.G., GUÉRIN, G., HAMAHASHI, M., HOUSE, B.M., HÜPERS, A., JEPSON,
907 T.N., KENIGSBERG, A.R., KURANAGA, M., NAIR, N., OWARI, S., SHAN, Y., SONG, I.,
908 TORRES, M.E., VANNUCCHI, P., VROLIJK, P.J., YANG, T., ZHAO, X. & THOMAS, E. (2017)
909 Understanding Himalayan Erosion and the Significance of the Nicobar Fan. *Earth and
910 Planetary Science Letters*, **475**, 134-142. doi:10.1016/j.epsl.2017.07.019.

- 911 MCQUARRIE, N., ROBINSON, D., LONG, S., TOBGAY, T., GRUJIC, D., GEHRELS, G. & DUCEA, M.
 912 (2008) Preliminary Stratigraphic and Structural Architecture of Bhutan: Implications for
 913 the Along Strike Architecture of the Himalayan System. *Earth and Planetary Science*
 914 *Letters*, **272**, 105-117. doi:10.1016/j.epsl.2008.04.030.
- 915 MEIGS, A.J., BURBANK, D.W. & BECK, R.A. (1995) Middle-Late Miocene (>10 Ma) Formation of
 916 the Main Boundary Thrust in the Western Himalaya. *Geology*, **23**, 423-426.
 917 doi:10.1130/0091-7613(1995)023<0423:MLMMFO>2.3.CO;2.
- 918 MILLER, C., KLÖTZLI, U., FRANK, W., THÖNI, M. & GRASEMANN, B. (2000) Proterozoic Crustal
 919 Evolution in the Nw Himalaya (India) as Recorded by Circa 1.80 Ga Mafic and 1.84 Ga
 920 Granitic Magmatism. *Precambrian Research*, **103**, 191-206. doi:10.1016/S0301-
 921 9268(00)00091-7.
- 922 MILLER, C., THÖNI, M., FRANK, W., GRASEMANN, B., KLÖTZLI, U., GUNTLI, P. & DRAGANITS, E.
 923 (2001) The Early Palaeozoic Magmatic Event in the Northwest Himalaya, India: Source,
 924 Tectonic Setting and Age of Emplacement. *Geological Magazine*, **138**, 237-251.
 925 doi:10.1017/s0016756801005283.
- 926 MOLNAR, P., ENGLAND, P. & MARTINOD, J. (1993) Mantle Dynamics, Uplift of the Tibetan
 927 Plateau, and the Indian Monsoon. *Reviews of Geophysics*, **31**, 357-396.
 928 doi:10.1029/93RG02030.
- 929 MOLNAR, P. & STOCK, J.M. (2009) Slowing of India's Convergence with Eurasia since 20 Ma and
 930 Its Implications for Tibetan Mantle Dynamics. *Tectonics*, **28**. doi:10.1029/2008TC002271.
- 931 MURPHY, M.A. & YIN, A. (2003) Structural Evolution and Sequence of Thrusting in the Tethyan
 932 Fold-Thrust Belt and Indus-Yalu Suture Zone, Southwest Tibet. *GSA Bulletin*, **115**, 21-34.
 933 doi:10.1130/0016-7606(2003)115<0021:Seasot>2.0.Co;2.
- 934 MYROW, P.M., HUGHES, N.C., PAULSEN, T.S., WILLIAMS, I.S., PARCHA, S.K., THOMPSON, K.R.,
 935 BOWRING, S.A., PENG, S.C. & AHLUWALIA, A.D. (2003) Integrated Tectonostratigraphic
 936 Analysis of the Himalaya and Implications for Its Tectonic Reconstruction. *Earth and*
 937 *Planetary Science Letters*, **212**, 433-441. doi:10.1016/s0012-821x(03)00280-2.
- 938 MYROW, P.M., HUGHES, N.C., GOODGE, J.W., FANNING, C.M., WILLIAMS, I.S., PENG, S.,
 939 BHARGAVA, O.N., PARCHA, S.K. & POGUE, K.R. (2010) Extraordinary Transport and
 940 Mixing of Sediment across Himalayan Central Gondwana During the Cambrian-
 941 Ordovician. *Geological Society of America Bulletin*, **122**, 1660-1670.
 942 doi:10.1130/b30123.1.
- 943 MYROW, P.M., HUGHES, N.C., DERRY, L.A., MCKENZIE, R.N., JIANG, G., WEBB, A.A.G.,
 944 BANERJEE, D.M., PAULSEN, T.S. & SINGH, B.P. (2015) Neogene Marine Isotopic Evolution
 945 and the Erosion of Lesser Himalayan Strata: Implications for Cenozoic Tectonic History.
 946 *Earth and Planetary Science Letters*, **417**, 142-150. doi:10.1016/j.epsl.2015.02.016.
- 947 NAJMAN, Y., JOHNSON, K., WHITE, N. & OLIVER, G. (2004) Evolution of the Himalayan Foreland
 948 Basin, Nw India. *Basin Research*, **16**, 1-24. doi:10.1111/j.1365-2117.2004.00223.x.
- 949 NAJMAN, Y. (2006) The Detrital Record of Orogenesis: A Review of Approaches and Techniques
 950 Used in the Himalayan Sedimentary Basins. *Earth-Science Reviews*, **74**, 1 –72.
 951 doi:10.1016/j.earscirev.2005.04.004.
- 952 NAJMAN, Y., BICKLE, M., GARZANTI, E., PRINGLE, M., BARFOD, D., BROZOVIC, N., BURBANK, D. &
 953 ANDO, S. (2009) Reconstructing the Exhumation History of the Lesser Himalaya, Nw
 954 India, from a Multitechnique Provenance Study of the Foreland Basin Siwalik Group.
 955 *Tectonics*, **28**, n/a-n/a. doi:10.1029/2009tc002506.
- 956 NAJMAN, Y., BICKLE, M., GARZANTI, E., PRINGLE, M., BARFOD, D., BROZOVIC, N., BURBANK, D. &
 957 ANDO, S. (2010) Correction to “Reconstructing the Exhumation History of the Lesser

- 958 Himalaya, Nw India, from a Multitechnique Provenance Study of the Foreland Basin
 959 Siwalik Group". *Tectonics*, **29**. doi:10.1029/2010TC002778.
- 960 NAJMAN, Y., JENKS, D., GODIN, L., BOUDAGHER-FADEL, M., MILLAR, I., GARZANTI, E.,
 961 HORSTWOOD, M. & BRACCIALI, L. (2017) The Tethyan Himalayan Detrital Record Shows
 962 That India–Asia Terminal Collision Occurred by 54 Ma in the Western Himalaya. *Earth
 963 and Planetary Science Letters*, **459**, 301-310. doi:10.1016/j.epsl.2016.11.036.
- 964 NESBITT, H.W., MARKOVICS, G. & PRICE, R.C. (1980) Chemical Processes Affecting Alkalis and
 965 Alkaline Earths During Continental Weathering. *Geochimica et Cosmochimica Acta*, **44**,
 966 1659–1666. doi:10.1016/0016-7037(80)90218-5.
- 967 PARKASH, B., SHARMA, R.P. & ROY, A.K. (1980) The Siwalik Group (Molasses)–Sediments Shed
 968 by Collision of Continental Plates. *Sedimentary Geology*, **25**, 127–159. doi:10.1016/0037-
 969 0738(80)90058-5.
- 970 PARRISH, R.R. & HODGES, V. (1996) Isotopic Constraints on the Age and Provenance of the Lesser
 971 and Greater Himalayan Sequences, Nepalese Himalaya. *Geological Society of America
 972 Bulletin*, **108**, 904-911. doi:10.1130/0016-7606(1996)108<0904:icotaa>2.3.Co;2.
- 973 PRELL, W.L. & KUTZBACH, J.E. (1992) Sensitivity of the Indian Monsoon to Forcing Parameters
 974 and Implications for Its Evolution. *Nature*, **360**, 647-652. doi:10.1038/360647a0.
- 975 PRELL, W.L., MURRAY, D.W., CLEMENS, S.C. & ANDERSON, D.M. (1992) Evolution and
 976 Variability of the Indian Ocean Summer Monsoon: Evidence from the Western Arabian
 977 Sea Drilling Program. In: *Synthesis of Results from Scientific Drilling in the Indian Ocean*
 978 (Ed. by R. A. Duncan, D. K. Rea, R. B. Kidd, U. von Rad & J. K. Weissel), *Geophysical
 979 Monograph*, **70**, 447–469. American Geophysical Union, Washington, DC.
- 980 QUADE, J., CERLING, T.E. & BOWMAN, J.R. (1989) Development of Asian Monsoon Revealed by
 981 Marked Ecological Shift During the Latest Miocene in Northern Pakistan. *Nature*, **342**,
 982 163-166. doi:10.1038/342163a0.
- 983 RAVIKANT, V., WU, F.-Y. & JI, W.-Q. (2011) U–Pb Age and Hf Isotopic Constraints of Detrital
 984 Zircons from the Himalayan Foreland Subathu Sub-Basin on the Tertiary Palaeogeography
 985 of the Himalaya. *Earth and Planetary Science Letters*, **304**, 356-368.
 986 doi:10.1016/j.epsl.2011.02.009.
- 987 RICHARDS, A., ARGELS, T., HARRIS, N., PARRISH, R., AHMAD, T., DARBYSHIRE, F. & DRAGANTIS,
 988 E. (2005) Himalayan Architecture Constrained by Isotopic Tracers from Clastic Sediments.
 989 *Earth and Planetary Science Letters*, **236**, 773-796. doi:10.1016/j.epsl.2005.05.034.
- 990 ROBERT, X., VAN DER BEEK, P., BRAUN, J., PERRY, C. & MUGNIER, J.-L. (2011) Control of
 991 Detachment Geometry on Lateral Variations in Exhumation Rates in the Himalaya:
 992 Insights from Low-Temperature Thermochronology and Numerical Modeling. *Journal of
 993 Geophysical Research: Solid Earth*, **116**. doi:10.1029/2010JB007893.
- 994 ROBINSON, D.M., DECELLES, P.G., PATCHETT, P.J. & GARZIONE, C.N. (2001) The Kinematic
 995 Evolution of the Nepalese Himalaya Interpreted from Nd Isotopes. *Earth and Planetary
 996 Science Letters*, **192**, 507-521. doi:10.1016/S0012-821X(01)00451-4.
- 997 ROBINSON, D.M., DECELLES, P.G. & COPELAND, P. (2006) Tectonic Evolution of the Himalayan
 998 Thrust Belt in Western Nepal; Implications for Channel Flow Models. *Geological Society
 999 of America Bulletin*, **118**, 865-885. doi:10.1130/B25911.1.
- 1000 SAHNI, A. & SRIVASTAVA, V.C. (1976) Eocene Rodents and Associated Reptiles from the Subathu
 1001 Formation of Northwestern India. *Journal of Paleontology*, **50**, 922-928.
- 1002 SCHLUP, M., STECK, A., CARTER, A., COSCA, M., EPARD, J.-L. & HUNZIKER, J. (2011) Exhumation
 1003 History of the Nw Indian Himalaya Revealed by Fission Track and 40Ar/39Ar Ages.
 1004 *Journal of Asian Earth Sciences*, **40**, 334-350. doi:10.1016/j.jseas.2010.06.008.

- 1005 SCHWERTMANN, U. (1971) Transformation of Hematite to Goethite in Soils. *Nature*, **232**, 624–625.
- 1006 SINGH, P. (2009) Major, Trace and Ree Geochemistry of the Ganga River Sediments: Influence of
1007 Provenance and Sedimentary Processes. *Chemical Geology*, **266**, 242-255.
1008 doi:10.1016/j.chemgeo.2009.06.013.
- 1009 SINGH, S., PARKASH, B., AWASTHI, A.K. & KUMAR, S. (2011) Late Miocene Record of
1010 Palaeovegetation from Siwalik Palaeosols of the Ramnagar Sub-Basin, India. *Current
1011 Science*, **100**, 213-222.
- 1012 SINGH, T., AWASTHI, A.K. & CAPUTO, R. (2012) The Sub-Himalayan Fold-Thrust Belt in the 1905
1013 Kangra Earthquake Zone: A Critical Taper Model Perspective for Seismic Hazard
1014 Analysis. *Tectonics*, **31**. doi:10.1029/2012TC003120.
- 1015 SORKHABI, R.B. & ARITA, K. (1997) Toward a Solution for the Himalayan Puzzle: Mechanism of
1016 Inverted Metamorphism Constrained by the Siwalik Sedimentary Record. *Current Science*,
1017 **72**, 862-873.
- 1018 STECK, A. (2003) Geology of the Nw Indian Himalaya. *Eclogae Geol Helv*, **96**, 147-196.
- 1019 STEVENS, V.L. & AVOUAC, J.P. (2015) Interseismic Coupling on the Main Himalayan Thrust.
1020 *Geophysical Research Letters*, **42**, 5828-5837. doi:10.1002/2015GL064845.
- 1021 STÜBNER, K., GRUJIC, D., DUNKL, I., THIEDE, R. & EUGSTER, P. (2018) Pliocene Episodic
1022 Exhumation and the Significance of the Munsiri Thrust in the Northwestern Himalaya.
1023 *Earth and Planetary Science Letters*, **481**, 273-283. doi:10.1016/j.epsl.2017.10.036.
- 1024 SUNDELL, K. & SAYLOR, J.E. (2017) Unmixing Detrital Geochronology Age Distributions.
1025 *Geochemistry Geophysics Geosystems*, **18**, 2872–2886. doi:10.1002/2016GC006774.
- 1026 TEWARI, V. (2003) Sedimentology, Palaeobiology and Stable Isotope Chemostratigraphy of the
1027 Terminal Neoproterozoic Buxa Dolomite, Arunachal Pradesh, Ne Lesser Himalaya.
1028 *Journal of Himalayan Geology*, **18**, 1–18.
- 1029 THAKUR, S.S. & TRIPATHI, K. (2008) Regional Metamorphism in the Haimanta Group of Rocks,
1030 Sutlej River Valley, Nw Himalaya, India. *Current Science*, **95**, 104-109.
- 1031 THAKUR, V.C., JAYANGONDAPERUMAL, R. & MALIK, M.A. (2010) Redefining Medlicott–Wadia's
1032 Main Boundary Fault from Jhelum to Yamuna: An Active Fault Strand of the Main
1033 Boundary Thrust in Northwest Himalaya. *Tectonophysics*, **489**, 29-42.
1034 doi:10.1016/j.tecto.2010.03.014.
- 1035 THIEDE, R., ROBERT, X., STÜBNER, K., DEY, S. & FARUHN, J. (2017) Sustained out-of-Sequence
1036 Shortening Along a Tectonically Active Segment of the Main Boundary Thrust: The
1037 Dhauladhar Range in the Northwestern Himalaya. *Lithosphere*, **9**, 715-725.
1038 doi:10.1130/1630.1.
- 1039 THIEDE, R.C., BOOKHAGEN, B., ARROWSMITH, J.R., SOBEL, E.R. & STRECKER, M.R. (2004)
1040 Climatic Control on Rapid Exhumation Along the Southern Himalayan Front. *Earth and
1041 Planetary Science Letters*, **222**, 791-806. doi:10.1016/j.epsl.2004.03.015.
- 1042 THIEDE, R.C., EHLERS, T.A., BOOKHAGEN, B. & STRECKER, M.R. (2009) Erosional Variability
1043 Along the Northwest Himalaya. *Journal of Geophysical Research*, **114**.
1044 doi:10.1029/2008JF001010.
- 1045 THIEDE, R.C. & EHLERS, T.A. (2013) Large Spatial and Temporal Variations in Himalayan
1046 Denudation. *Earth and Planetary Science Letters*, **374**, 256-257.
1047 doi:10.1016/j.epsl.2013.03.004.
- 1048 VALDIYA, K. (1980) Geology of Kumaun Lesser Himalaya, Wadia Institute of Himalayan
1049 Geology. Dehradun, India, 1-291.
- 1050 VAN DER BEEK, P., ROBERT, X., MUGNIER, J.-L., BERNET, M., HUYGHE, P. & LABRIN, E. (2006)
1051 Late Miocene-Recent Exhumation of the Central Himalaya and Recycling in the Foreland

- 1052 Basin Assessed by Apatite Fission-Track Thermochronology of Siwalik Sediments, Nepal.
 1053 *Basin Research*, **18**, 413–434. doi:10.1111/j.1365-2117.2006.00305.x.
- 1054 VAN HINSBERGEN, D.J.J., LIPPERT, P.C., DUPONT-NIVET, G., MCQUARRIE, N., DOUBROVINE, P.V.,
 1055 SPAKMAN, W. & TORSVIK, T.H. (2012) Greater India Basin Hypothesis and a Two-Stage
 1056 Cenozoic Collision between India and Asia. *Proceedings Of The National Academy of*
 1057 *Sciences*, **109**, 7659–7664. doi:10.1073/pnas.1117262109.
- 1058 VANNAY, J. & GRASEMANN, B. (1998) Inverted Metamorphism in the High Himalaya of Himachal
 1059 Pradesh (Nw India): Phase Equilibria Versus Thermobarometry. *Schweizerische*
 1060 *Mineralogische und Petrographische Mitteilungen*, **78**, 107–132.
- 1061 VANNAY, J.-C., GRASEMANN, B., RAHN, M., FRANK, W., CARTER, A., BAUDRAZ, V. & COSCA, M.
 1062 (2004) Miocene to Holocene Exhumation of Metamorphic Crustal Wedges in the Nw
 1063 Himalaya: Evidence for Tectonic Extrusion Coupled to Fluvial Erosion. *Tectonics*, **23**.
 1064 doi:10.1029/2002TC001429.
- 1065 VERMEESCH, P. (2013) Multi-Sample Comparison of Detrital Age Distributions. *Chemical*
 1066 *Geology*, **341**, 140–146. doi:10.1016/j.chemgeo.2013.01.010.
- 1067 VÖGELI, N., NAJMAN, Y., VAN DER BEEK, P., HUYGHE, P., WYNN, P.M., GOVIN, G., VEEN, I.V.D. &
 1068 SACHSE, D. (2017a) Lateral Variations in Vegetation in the Himalaya since the Miocene
 1069 and Implications for Climate Evolution. *Earth and Planetary Science Letters*, **471**, 1–9.
 1070 doi:10.1016/j.epsl.2017.04.037.
- 1071 VÖGELI, N., VAN DER BEEK, P., HUYGHE, P. & NAJMAN, Y. (2017b) Weathering in the Himalaya,
 1072 an East-West Comparison: Indications from Major Elements and Clay Mineralogy. *The*
 1073 *Journal of Geology*, **125**, 515–529. doi: 10.1086/692652.
- 1074 WEBB, A.A.G. (2013) Preliminary Palinspastic Reconstruction of Cenozoic Deformation across
 1075 the Himachal Himalaya (Northwestern India). *Geosphere*, **9**, 572–587.
 1076 doi:10.1130/GES00787.1.
- 1077 WEST, A.J., GALY, A. & BICKLE, M.J. (2005) Tectonic and Climatic Controls on Silicate
 1078 Weathering. *Earth and Planetary Science Letters*, **235**, 211–228. doi:
 1079 10.1016/j.epsl.2005.03.020.
- 1080 WHITE, N.M., PARRISH, R.R., BICKLE, M.J., NAJMAN, Y.M.R., BURBANK, D.W. & MAITHANI, A.
 1081 (2001) Metamorphism and Exhumation of the Nw Himalaya Constrained by U-Th-Pb
 1082 Analysis of Detrital Monazite Grains from Early Foreland Basin. *Journal of the Geological*
 1083 *Society*, **158**, 625–635. doi:10.1144/jgs.158.4.625.
- 1084 WHITE, N.M., PRINGLE, M., GARZANTI, E., BICKLE, M., NAJMAN, Y., CHAPMAN, H. & FRIEND, P.
 1085 (2002) Constraints on the Exhumation and Erosion of the High Himalayan Slab, Nw India,
 1086 from Foreland Basin Deposits. *Earth and Planetary Science Letters*, **195**, 29–44.
 1087 doi:10.1016/s0012-821x(01)00565-9.
- 1088 WILLETT, S.D., FISHER, D., FULLER, C., YEH, E.-C. & LU, C.-Y. (2003) Erosion Rates and
 1089 Orogenic-Wedge Kinematics in Taiwan Inferred from Fission-Track Thermochronometry.
 1090 *Geology*, **31**, 945–948. doi:10.1130/g19702.1.
- 1091 WOBUS, C.W., HODGES, K.V. & WHIPPLE, K.X. (2003) Has Focused Denudation Sustained Active
 1092 Thrusting at the Himalayan Topographic Front? *Geology*, **31**, 861–864.
- 1093 WU, F.Y., JI, W.Q., WANG, J.G., LIU, C.Z., CHUNG, S.L. & CLIFT, P.D. (2014) Zircon U-Pb and Hf
 1094 Isotopic Constraints on the Onset Time of India-Asia Collision. *American Journal of*
 1095 *Science*, **314**, 548–579. doi:10.2475/02.2014.04].
- 1096 YIN, A. (2006) Cenozoic Tectonic Evolution of the Himalayan Orogen as Constrained by Along-
 1097 Strike Variation of Structural Geometry, Exhumation History, and Foreland Sedimentation.
 1098 *Earth-Science Reviews*, **76**, 1–131. doi:10.1016/j.earscirev.2005.05.004.

- 1099 ZHOU, P., CARTER, A., LI, Y. & CLIFT, P.D. (2020) Slowing Rates of Regional Exhumation in the
1100 Western Himalaya: Fission Track Evidence from the Indus Fan. *Geological Magazine*,
1101 **157**, 848-863. doi:10.1017/S0016756819000608.
- 1102 ZHOU, P., IRELAND, T., MURRAY, R.W. & CLIFT, P.D. (2021) Marine Sedimentary Records of
1103 Chemical Weathering Evolution in the Western Himalaya since 17 Ma. *Geosphere*, **17**.
1104 doi:10.1130/GES02211.1.
1105
- 1106

1107 **Figure and Table Captions**

1108 **Figure 1.** Geological map of the Western Himalayas showing the major tectonic units that are
1109 eroded by the Indus River and its tributaries. Map is modified after Alizai *et al.* (2011). Rivers are
1110 shown in thick black lines. ISZ – Indus Suture Zone, MCT – Main Central Thrust, MBT – Main
1111 Boundary Thrust and MFT – Main Frontal Thrust. Sample locations are shown as filled red dots.
1112 JW – Jawalamukhi and JN – Joginder Nagar.

1113 **Figure 2. (A)** Topographic map of the Northwestern Himalayas made with ArcGIS Software from
1114 NASA’s Shuttle Radar Topography Mission (SRTM). Red boxes show the location of the detailed
1115 study areas. Map also shows the primary source ranges, major fault systems, and reentrant zones
1116 after Singh *et al.* (2012). Palampur Thrust is from Thakur *et al.* (2010). ILH – Inner Lesser
1117 Himalayas, OLH – Outer Lesser Himalayas, GHS – Greater Himalayas, THS – Tethyan Himalayas,
1118 SH – Sub-Himalayas, MCT – Main Central Thrust, MBT – Main Boundary Thrust and MFT – Main
1119 Frontal Thrust, and TZ – Transition Zone. The TZ marks the transition between the Kangra and
1120 Nahan Salient Reentrants. **(B)** Sample locations for the Jawalamukhi section and **(C)** from the
1121 Joginder Nagar section on shaded SRTM topography plotted with GeoMapApp within the Kangra
1122 Reentrant.

1123
1124 **Figure 3.** Stratigraphic columns of the two foreland basin sections discussed in the text. The
1125 stratigraphic columns show thickness, lithology, and depositional ages for the Joginder Nagar (left)
1126 and the Jawalamukhi (right) sections. The depositional ages are derived from magnetostratigraphy
1127 (Meigs *et al.*, 1995). The Joginder Nagar section is modified from White *et al.* (2002) and the
1128 Jawalamukhi section is modified from Najman *et al.* (2009). Note the significant coarsening up in
1129 the Jawalamukhi section after 9 Ma.

1130

1131 **Figure 4.** (A) Geochemical signature of the analyzed samples (green symbols) illustrated by a
1132 CaO+Na₂O-Al₂O₃-K₂O (CN-A-K) ternary diagram (Fedo *et al.*, 1995), together with data from
1133 Vögeli *et al.* (2017b)(orange symbols) from the same section. CaO* represents the CaO associated
1134 with silicate, excluding all the carbonate. Samples closer to Al₂O₃ are rich in kaolinite, chlorite
1135 and/or gibbsite (representing by kao, chl and gib). CIA values are also calculated and shown on the
1136 left side, with its values are correlated with the CN-A-K. Abbreviations: sm (smectite), pl
1137 (plagioclase), ksp (K-feldspar), il (illite), m (muscovite). Quaternary Indus delta are from Clift *et*
1138 *al.* (2010), Holocene Indus Canyon data are from Li *et al.* (2018). Neogene Indus shelf and fan
1139 data are from Zhou *et al.* (2021). B) Geochemical classification of sediments from this study
1140 following the scheme of Herron (1988).

1141

1142 **Figure 5.** Kernel density estimate (KDE) plots for the zircon U–Pb ages from the foreland sections
1143 compared with some of the major source terrains and modern Indus River tributaries, as well the
1144 Yamuna in the Western Himalayas. Bedrock compilation is from Alizai *et al.* (2011), Cawood *et al.*
1145 (2007), DeCelles *et al.* (2004), Gehrels *et al.* (2011), Horton *et al.* (2013), Jonell *et al.* (2017), Kohn
1146 *et al.* (2009), McKenzie *et al.* (2011), Myrow *et al.* (2010), Martin *et al.* (2005; 2009), McQuarrie
1147 *et al.* (2008), Miller *et al.* (2001), Parrish *et al.* (1996). Major Indus River tributaries compilation is
1148 from Alizai *et al.* (2011). Colored strips highlight provenance diagnostic age populations: Purple –
1149 400–750 Ma, Blue – 750–900 Ma, Green – 900–1250 Ma, Brown – 1700–2000 Ma.

1150

1151 **Figure 6.** A) Multi-dimensional scalar (MDS) plot comparing the detrital samples from the
1152 Jawalamukhi and Joginder Nagar sections (yellow dots) with potential bedrock sources (red dots)

1153 and major Indus River tributaries (blue dots). ILH – Inner Lesser Himalayas, OLH – Outer Lesser
1154 Himalayas, GHS – Greater Himalayas, and THS – Tethyan Himalayas. Data sources are as for
1155 Figure 4. Note the progressive migration away from the OLH, THS, and GHS sources and towards
1156 the ILH source starting at the 7–8 Ma sample. B) Shows the same dataset without the extreme
1157 Indus and ILH outliers.

1158
1159 **Figure 7.** Lag time plot of detrital apatite fission track central ages showing the lag time between
1160 the cooling and depositional ages. Siwalik data from Karnali, Surai Khola and Tinau Khola
1161 (Nepal) are from van der Beek *et al.* (2006), Bengal Fan data is from Corrigan & Crowley (1990).
1162 Gray shaded area shows the range of time in this study area for which the samples are clearly reset
1163 for AFT. Samples from this study are all within error of the zero lag time line.

1164
1165 **Figure 8.** Calculated contributions from bedrock source terrains to sediments considered in this
1166 study through time based on the Kuiper unmixing calculations, compared with Nd isotope data
1167 from the same section from Najman *et al.* (2009) showing sediment matrix and conglomerate
1168 pebbles. Carbon isotopes from paleosols constrain vegetation and are from NW India (Vögeli *et*
1169 *al.*, 2017a) and the Potwar Plateau, Pakistan (Quade *et al.*, 1989). Hematite data from the Arabian
1170 Sea are from Zhou *et al.* (2021).

1171
1172 **Figure 9.** Kernel density estimate (KDE) plots for the zircon U–Pb ages from the foreland sections
1173 at Dehra Dun (Mandal *et al.*, 2019) and Jawalamukhi (this study) showing the relative loss of
1174 grains 400–1250 Ma after 8 Ma at the latter site while they continue to be an important component
1175 at the former.

1176
1177 **Figure 10.** Summary figure showing the evolving drainage exposure and migration of the two
1178 foreland sections towards the range front since 20 Ma with estimated outcrop patterns based on
1179 this and earlier studies showing the passage of the sections through different river flood plains
1180 through time. Modern map is based on DiPietro & Pogue (2004). UKW = Uttarkashi Window.
1181 Location of rivers is schematic and based on the provenance of the sediment constrained in this
1182 study.

1183
1184 **Table 1.** Locations of samples and estimated depositional ages based on magnetostratigraphy.
1185 Convergence rates are from Clark (2012).

1186
1187 **Table 2.** Major and select trace element geochemical analysis of the samples considered in this
1188 study. Major element concentrations are in weight percent. Trace elements are shown as parts per
1189 million (ppm).

1190
1191 **Table 3.** Fission track analytical data
1192 (i). Track densities are ($\times 10^6$ tr cm^{-2}) numbers of tracks counted (N) shown in brackets;
1193 (ii). analyses by external detector method using 0.5 for the $4\pi/2\pi$ geometry correction factor;
1194 (iii). ages calculated using dosimeter glass CN-5; (apatite) $\zeta_{\text{CN5}} = 339 \pm 5$;
1195 calibrated by multiple analyses of IUGS apatite and zircon age standards (Hurford, 1990);
1196 (iv). $P\chi^2$ is probability for obtaining χ^2 value for ν degrees of freedom, where $\nu = \text{no. crystals} - 1$;
1197 (v). Central age is a modal age, weighted for different precisions of individual crystals (Galbraith,
1198 1990).

1199

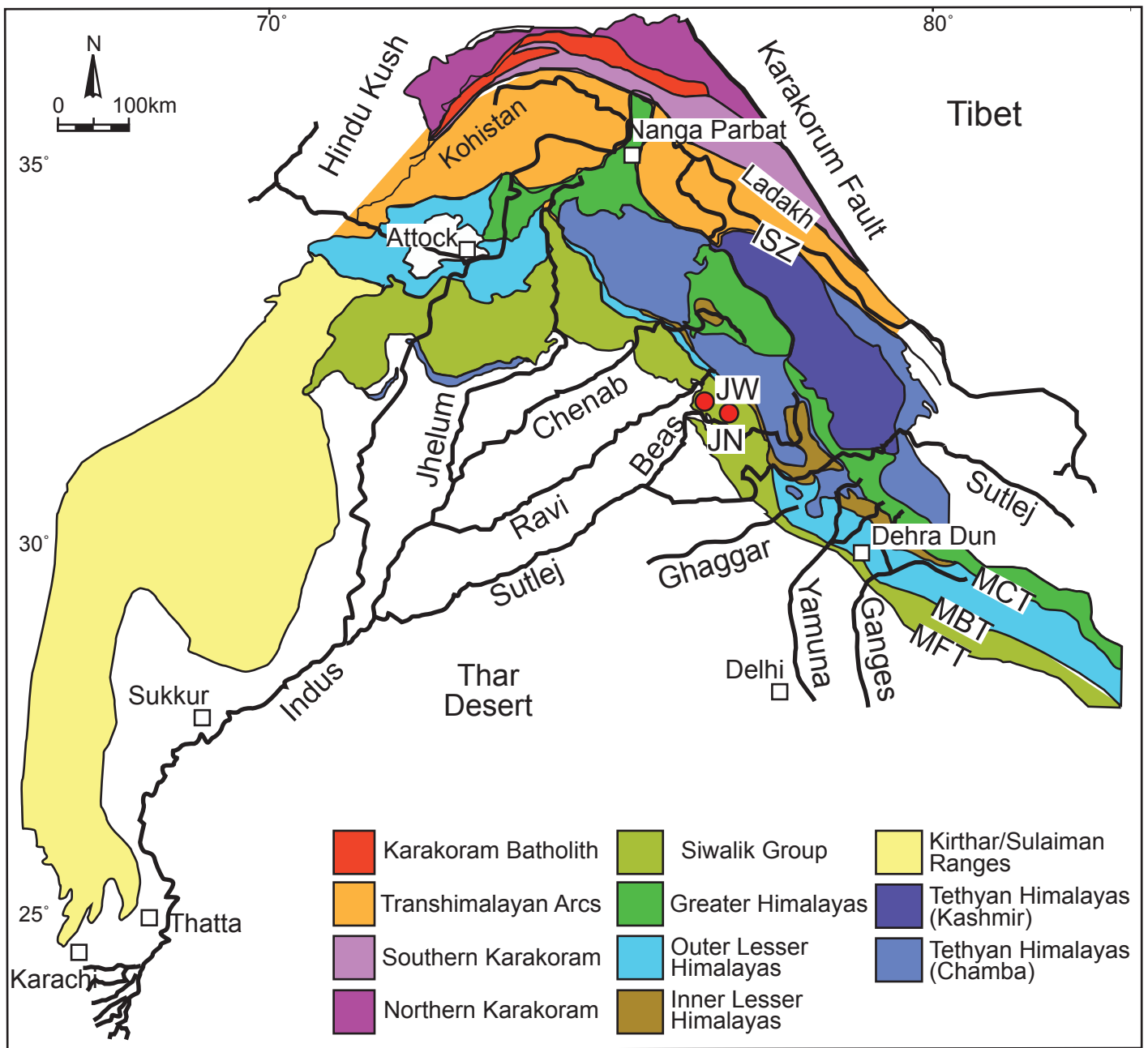


Figure 1
Exnicios et al.

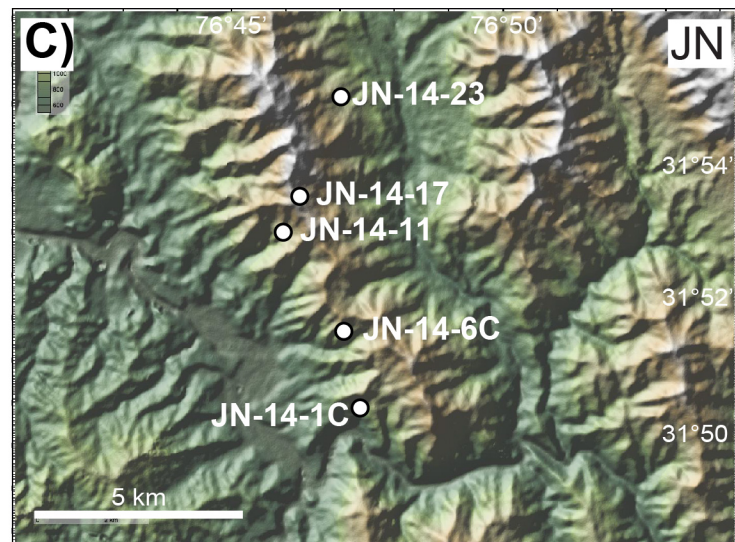
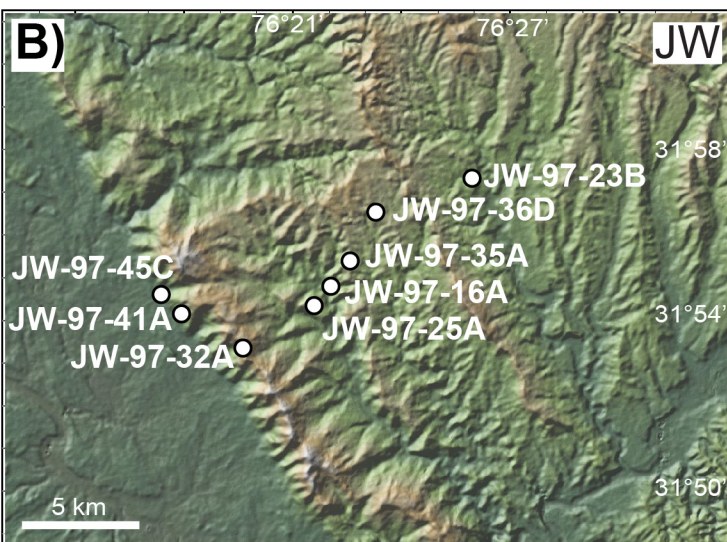
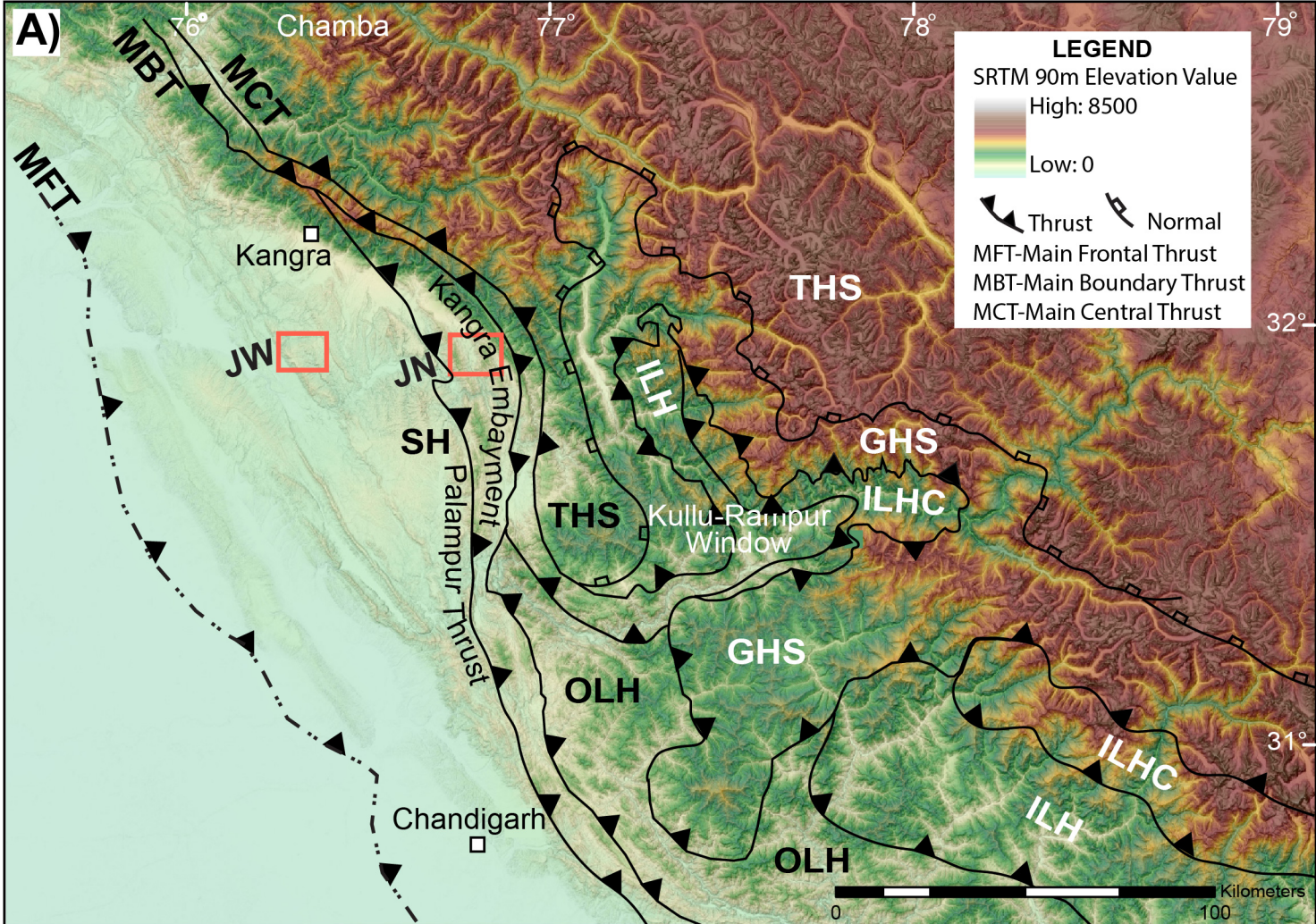


Figure 2
 Exnicios et al.

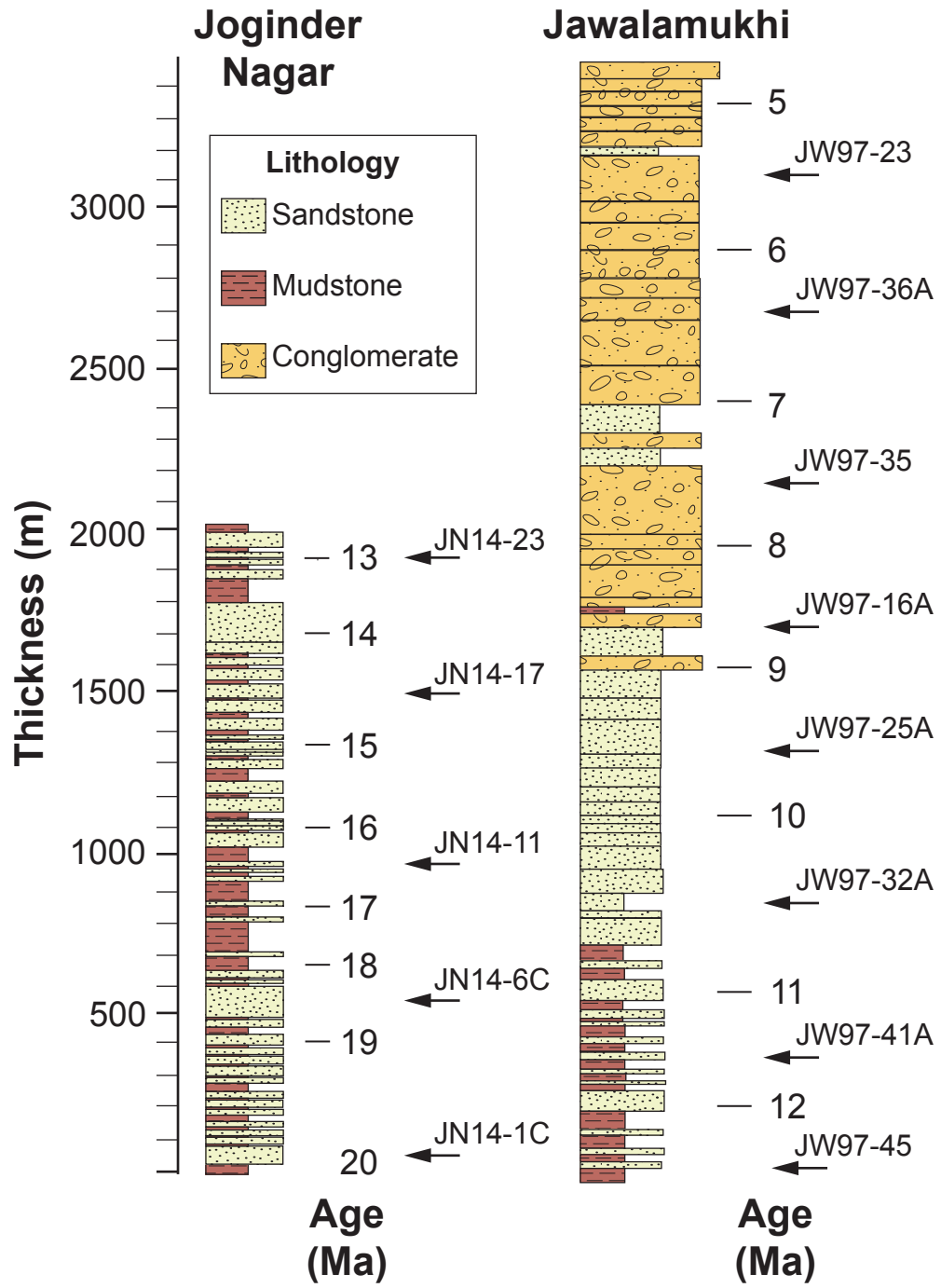


Figure 3
Exnicios et al.

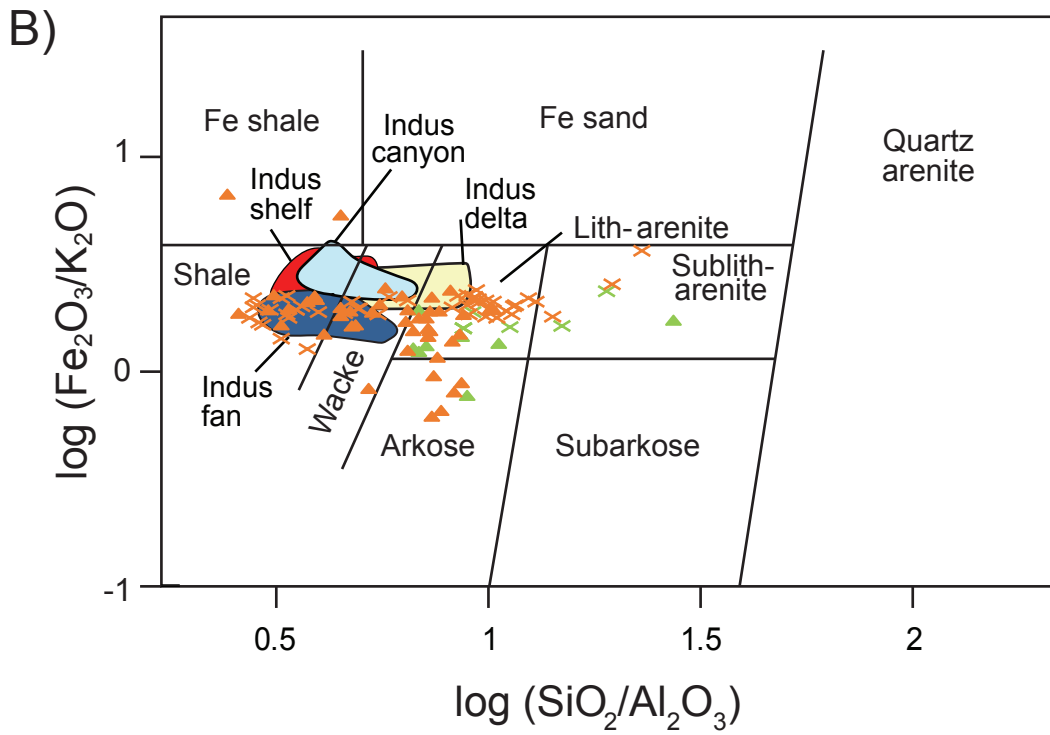
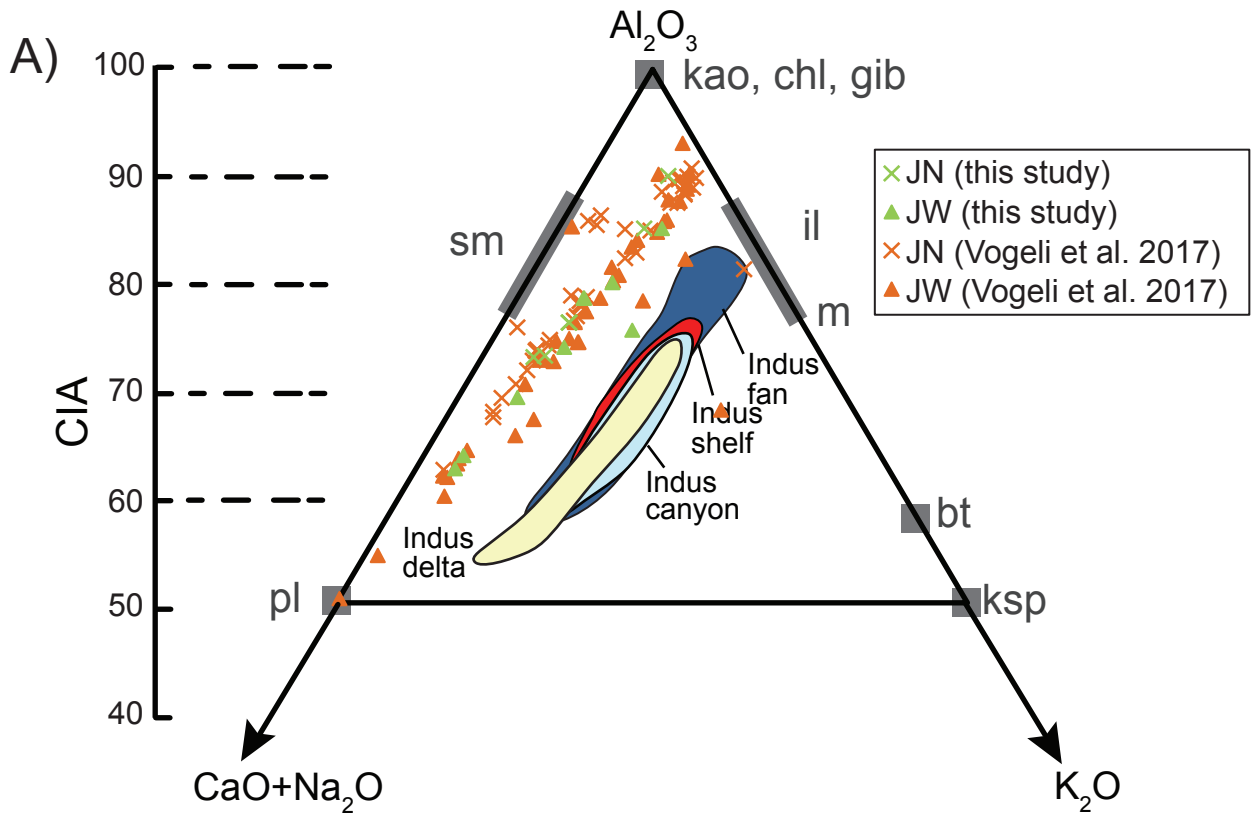


Figure 4
Exnicios et al.

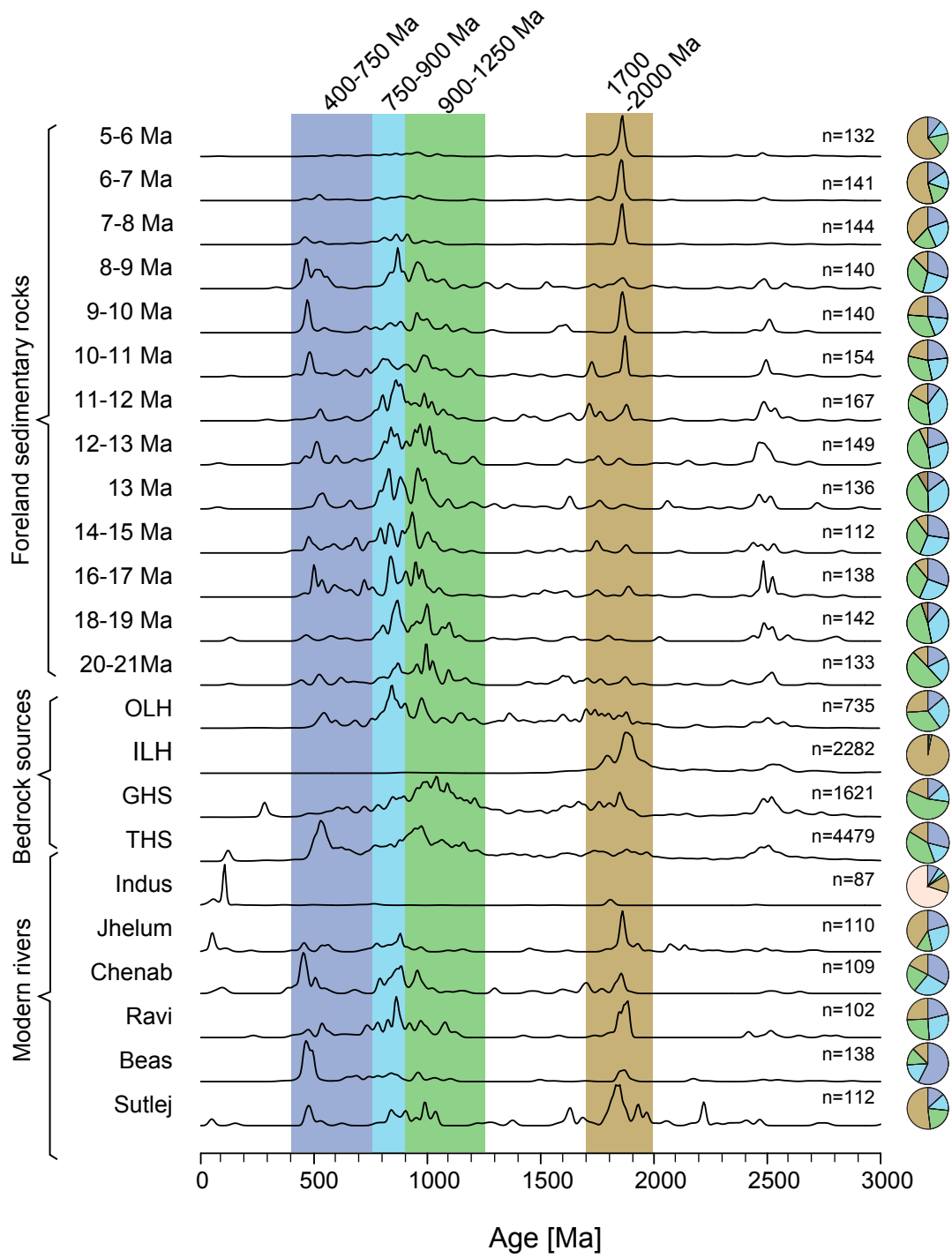


Figure 5
Exnicios et al.

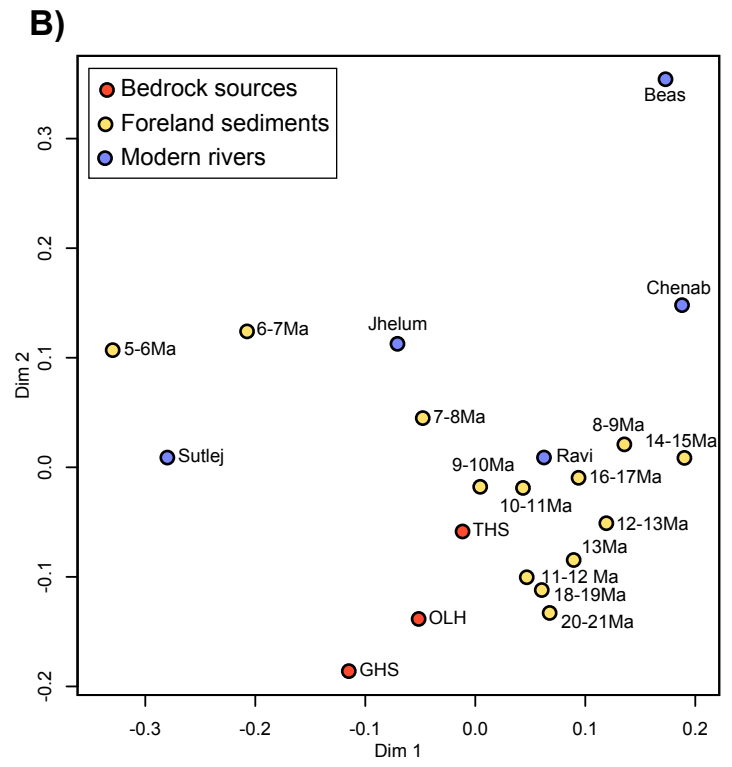
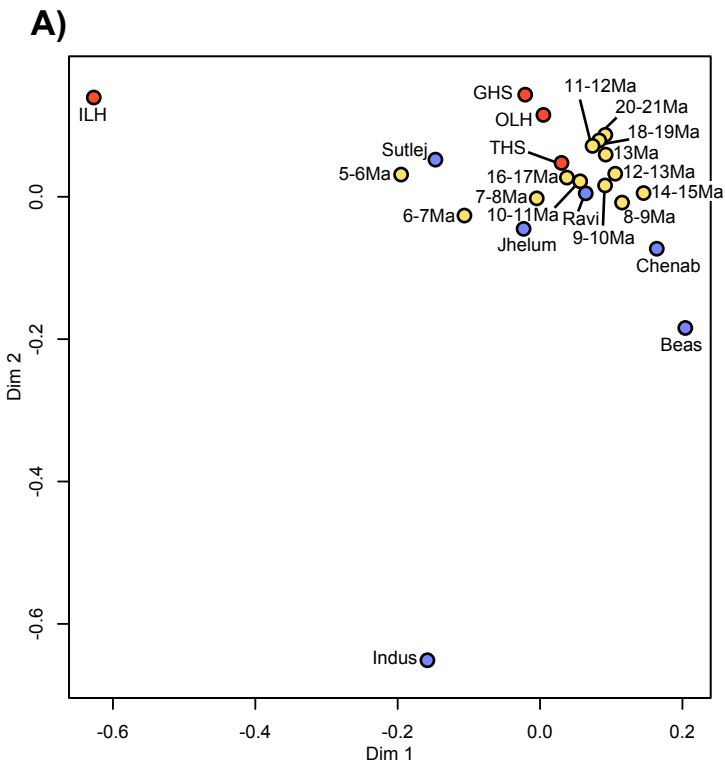


Figure 6
Exnicios et al.

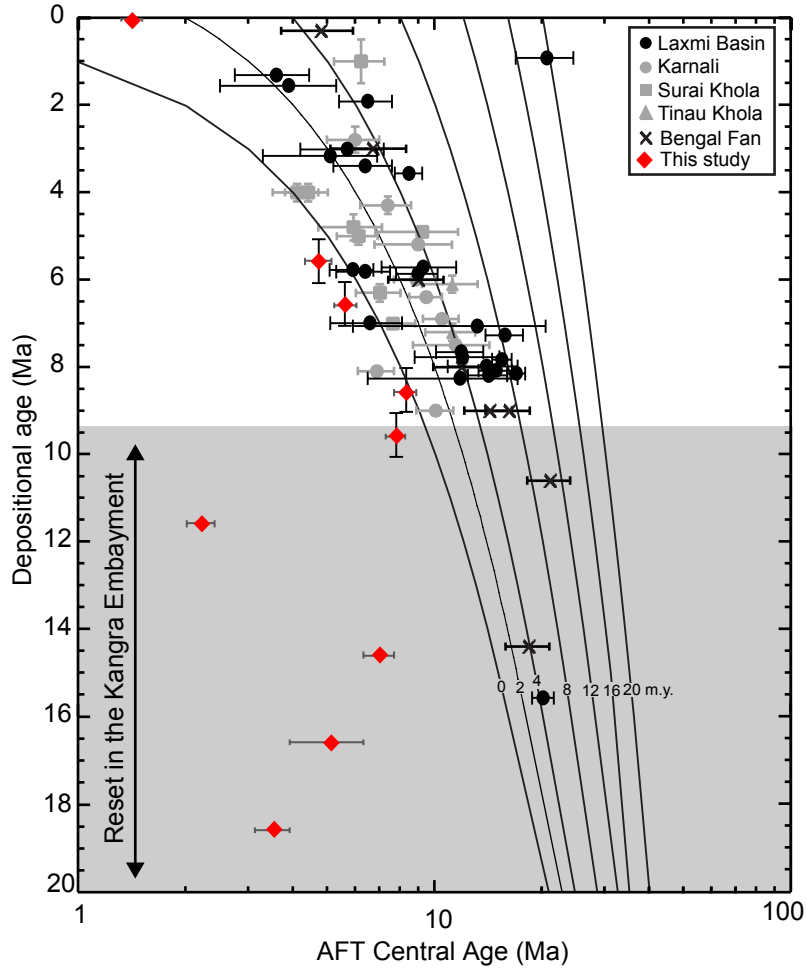


Figure 7
Exnicios et al.

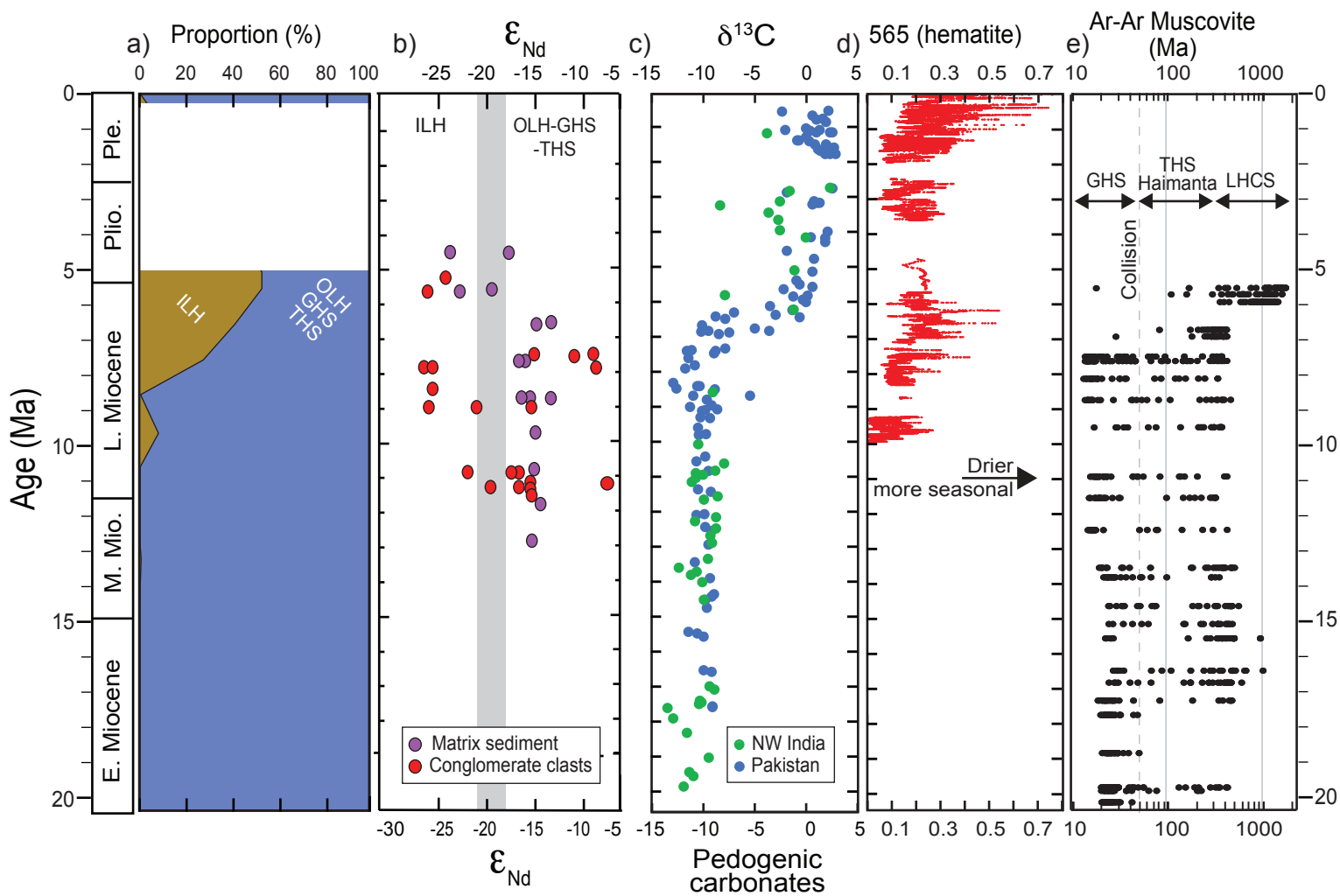


Figure 8
Exnicios et al.

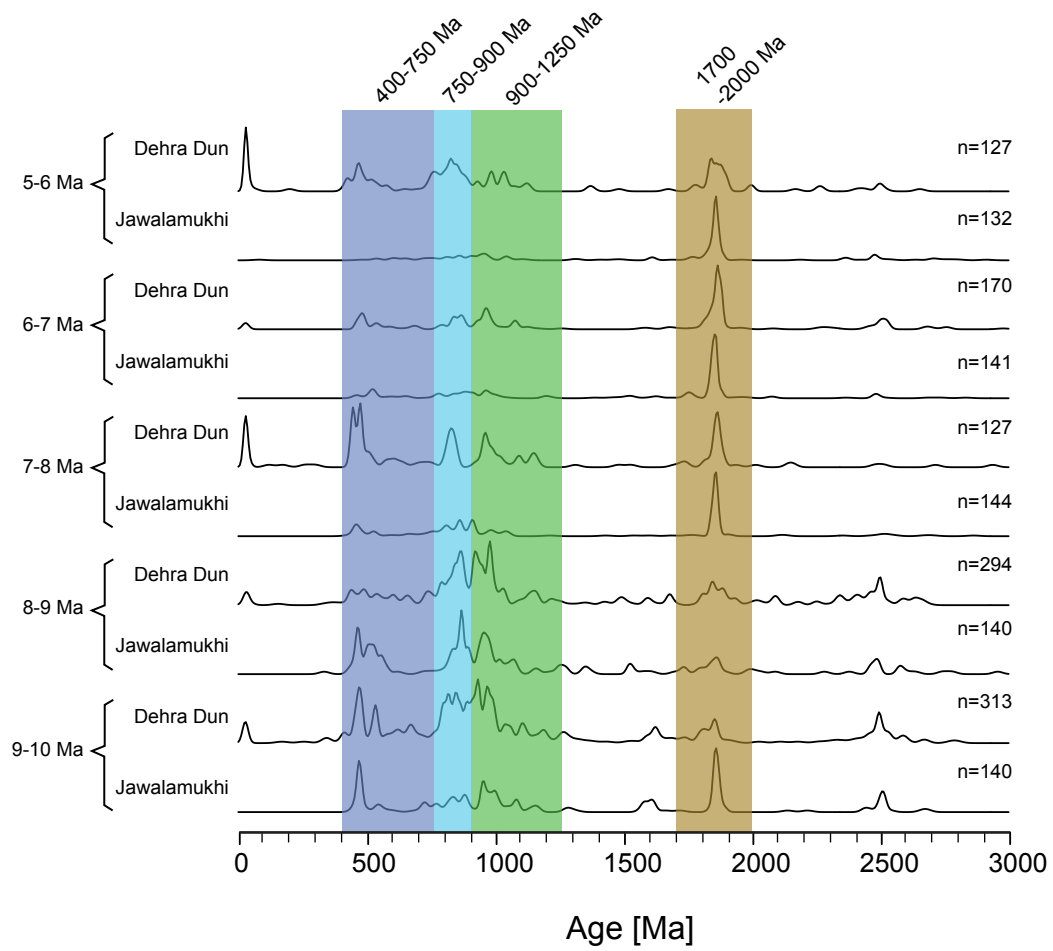


Figure 9
Exnicios et al.

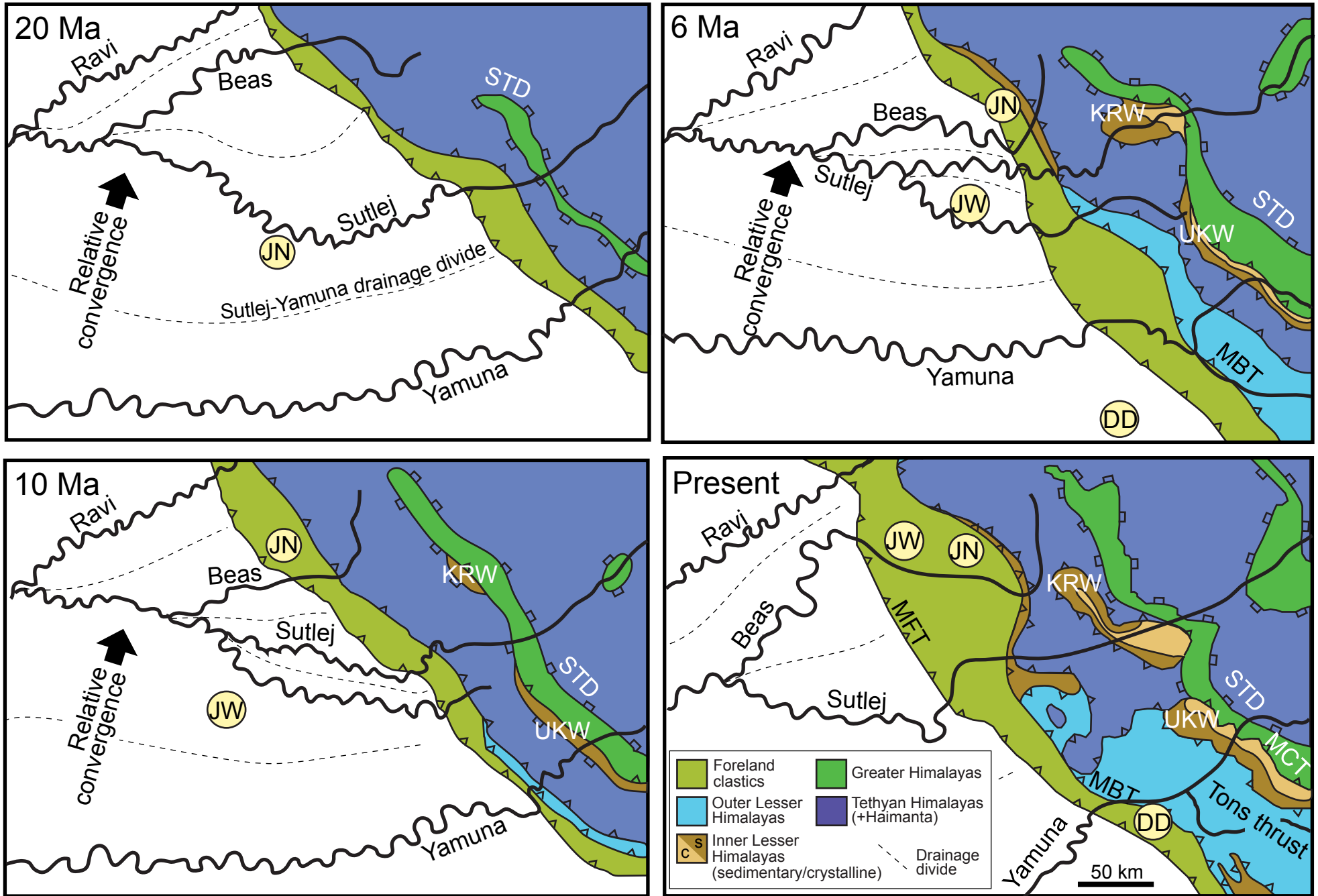


Figure 10
Exnicios et al.